Wide-Bandwidth Lasers and Modulators for RF Photonics

Nadir Dagli, *Member, IEEE*

(Invited Paper)

***Abstract*— In this paper, the basic principle of operation, design issues, limitations, recent developments and emerging research trends on wide-bandwidth lasers and modulators for radio-frequency photonic applications are reviewed. The topics covered are wide-bandwidth lasers, lumped and traveling-wave electroabsorption modulators, traveling-wave $LiNbO_3$, GaAs, and polymer modulators.**

***Index Terms*—Electroabsorption modulators, electrooptic polymer modulators, GaAs modulators, high-speed lasers, $LiNbO_3$ modulators, optical modulators, RF photonics, traveling-wave electrooptic modulators.**

I. Introduction

TRANSMISSION of analog microwave/millimeter-wave and high-speed digital signals over optical fibers is an enabling technology affecting many aspects of our lives. Very wide-bandwidth lasers and external optical modulators are essential components for this technology. The topic of this paper is lasers and modulators suitable for analog fiber-optic radio-frequency (RF) transmission or RF photonics. There are several important issues for RF photonics, which include link gain, noise figure, linearity, and spurious-free dynamic range. Some of these introduce stringent requirements for lasers and modulators. For example, the gain of a directly modulated link using a high-speed laser is proportional to S_L^2, where S_L is the external differential quantum efficiency of the directly modulated semiconductor laser [1]. A low-noise figure is another requirement, which, in turn, requires low-noise lasers. Very wide-bandwidth operation is clearly needed for microwave/millimeter-wave transmission.

Similarly, the gain of an externally modulated link using a Mach–Zehnder-type modulator is proportional to $(tP/V_\pi)^2$, where P is the input optical power, t is the fiber-to-fiber insertion loss, and V_π is the on/off switching voltage of the modulator [1]. In other types of modulators, tP/V_π should be replaced by an appropriate effective slope efficiency. This simple expression outlines some of the key requirements for modulators. Low V_π, capability of handling large amounts of optical power and low fiber-to-fiber insertion loss are essential to get high gain links. Linearity is another requirement for analog links. Almost all modulators have nonlinear transfer functions. As a result, the device is biased at specific points on the electrical-to-optical transfer function to assure linearity and a large intermodulation-free dynamic range. Therefore, linearity and the stability of the bias point are also very important. Very wide-bandwidth or high-speed operation is also essential for any microwave or millimeter-wave application. For many RF photonic applications, chirp is not a major concern, unless at very high frequencies, since distances involved are often usually much shorter than those in communication applications.

The remainder of this paper contains two major sections. Sections II and III are on wide-bandwidth lasers and modulators, respectively. Finally, a summary is given in Section IV. Each section starts with a brief tutorial, which is followed by the discussion of the design issues. Specific examples are then presented, along with a brief discussion of recent and emerging research directions.

II. Wide-Bandwidth Lasers

Limitations to high-speed operation of semiconductor lasers can be categorized in two groups. Considerations other than the active layer can be collected in one group. They include factors such as the design of the optical cavity, reduction of the parasitics, and efficient removal of the excess heat. On the other hand, intrinsic properties of the active layer present the ultimate limit on the speed of operation and has led to utilization of quantum wells (QW's). A recent detailed review of wide-bandwidth lasers can be found in [2].

Using rate equations, small-signal modulation response of a directly modulated semiconductor laser can be expressed as [2], [3]

$$H(\omega) = \frac{A}{\omega_r^2 - \omega^2 + j\omega\gamma} \tag{1}$$

where A is an amplitude factor, ω is the angular modulation frequency, $\omega_r = 2\pi f_r$ is the angular relaxation resonance frequency, and γ is the damping factor. f_r and the γ can be approximated as

$$f_r = \frac{1}{2\pi}\sqrt{\frac{v_g S_0}{\tau_p}} = \sqrt{\frac{v_g g_0 \Gamma \eta_i (I - I_{\rm th})}{qv}} \quad \gamma = g_0 S_0 + \frac{\varepsilon S_0}{\tau_p} \tag{2}$$

where S_0 is the steady-state photon density at the bias point, v_g is the group velocity, τ_p is the photon lifetime, g_0 is the differential gain, Γ is the optical confinement factor, η_i is the

Manuscript received November 10, 1998; revised March 22, 1999.

The author is with the Electrical and Computer Engineering Department, University of California at Santa Barbara, Santa Barbara, CA 93106 USA.

Publisher Item Identifier S 0018-9480(99)05185-6.

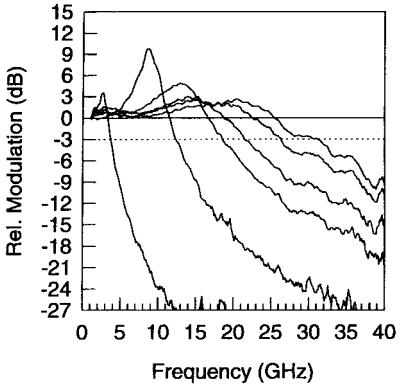

Fig. 1. Small-signal CW modulation response of a 6 × 130 μm^2 ridge waveguide laser at various bias currents (10, 20, 40, 60, 80, and 100 mA) [4, Fig. 1]. ©1995 IEEE.

internal quantum efficiency, v is the volume of the cavity, I is the bias current, $I_{\rm th}$ is the threshold current density, and ε is the nonlinear gain coefficient. As seen in (2), the damping factor and resonance frequency are related. Usually this relationship is expressed as

$$\gamma = Kf_r^2 + \gamma_0. \tag{3}$$

In practice, K (K factor) and γ_0 (damping factor offset) are experimentally obtained from the laser modulation response. This is done by experimentally determining γ and f_r from laser modulation response at different bias currents and plotting γ against f_r^2. The slope and intercept of this line yield K and γ_0, respectively. Fig. 1 shows the small-signal continuous wave (CW) modulation response of a high-speed laser, which is described later in this section [4]. From low to high frequencies, the response starts out flat, sharply peaks around f_r, and drops rather fast for frequencies extending beyond f_r. The amount of peaking depends on the relative magnitude of γ. As f_r increases, so does γ, and the response flattens out due to excessive damping. The maximum 3-dB bandwidth can be expressed as [5]

$$f_{\rm max} = \sqrt{2}\frac{2\pi}{K}. \tag{4}$$

Thus, the phenomenological K factor also determines the intrinsic bandwidth of the laser. High-modulation bandwidths require high f_r, which requires high differential gain, high optical power density, or high bias currents above threshold. Therefore, low $I_{\rm th}$ and high η_i are very important. Large photon densities require small cavity volumes or short and narrow optical waveguides for in-plane lasers. Strong index guiding in the optical waveguide is important to confine the optical mode to a narrow region. In this regard, ridge waveguide lasers, in which the waveguide is surrounded either by air or low dielectric constant dielectric, are commonly used. Typical lengths of lasers based on the InGaAs system are in the 100–150-μm range due to comparatively higher material gain. For InGaAsP-based lasers, lengths are of the order of 400 μm due to lower material gain. Furthermore, the laser should operate in the fundamental spatial mode not to partition the photon density among higher order modes and reduce the optical confinement. Therefore, high-speed lasers require short and narrow cavities with strong optical confinement.

For high-speed laser operation, material design is also very important. High differential gain, as well as low nonlinear gain saturation are required. High differential gain is typically obtained using QW's and strain. Compared to a bulk material, carrier density rises very sharply with carrier injection into a QW because of modified step-like density of states. In a laser, transparency is reached when the energy separation between the quasi-Fermi levels in the valence and conduction bands match the energy corresponding to the lasing wavelength. If the curvature of the conduction and valence bands is high, quasi-Fermi levels can move quite rapidly into the bands and transparency is reached with low carrier injection. In III–V compound semiconductors, this is typically the case for the conduction band. However, the valence band, especially the heavy hole (hh) band, has large curvature corresponding to a larger carrier effective mass. Introducing compressive strain into the QW lifts the degeneracy between the heavy and light hole (lh) bands, pushes the hh band closer to the conduction band, and increases its curvature. The effect of the strain on the conduction band is very slight. Therefore, compressive strain reduces the threshold current. At the same time, differential gain increases since changes in the carrier density with changing current is much higher. As current injected into the laser changes, so does the quasi-Fermi levels. Carrier density changes most rapidly at the energy of the quasi-Fermi levels due to the nature of Fermi function. Since the gain changes most rapidly at the band edges, if the quasi-Fermi levels are very close to the band edges, gain change with injected current, i.e., differential gain will be maximum [3]. Strain enables this and high differential gains result.

In the GaAs system, compressively strained QW's are grown by adding In. Typical In levels range between 10%–35%. In the InGaAsP system, it is possible to get both compressive and tensile strain, but compressive strain works better. In this case, combining compressive and tensile strain in the well and barrier overall stack can be built to yield overall zero strain. This is called strain compensation and enables large numbers of QW's. In the InGaAs system, strain keeps increasing with the overall thickness of the QW's and, typically, only four QW's are used.

On the other hand, nonlinear gain compression increases in strained material. The corresponding increase in the damping factor, in turn, limits the modulation bandwidth, as described earlier. Two processes contribute to the gain compression. One is the spectral hole burning caused by the depletion of carriers at and around the lasing energy. As carriers are depleted, gain is reduced, which dampens the response of the laser. Carriers consumed by lasing are supplied by injected carriers relaxing from their injection energies by intraband relaxation processes. These relaxation times can be reduced by increasing the carrier to carrier scattering rates, which can be achieved by p doping the active layer. The other contribution to the gain compression is carrier heating. Carriers at the band edge are constantly removed due to stimulated emission. Thus, the remaining distribution has an effective temperature higher than the lattice temperature, which reduces the differential

gain [6]. Carrier heating is higher for strained devices due to increased valence band curvature. Therefore, strained devices have higher damping rates.

Another very important consideration for the high-speed laser design is the transport related issues in the active region. Carrier transport inside the active region is quite complicated and involves diffusion of carriers from the edge of the separate confinement heterostructure (SCH) region, their capture and escape from the QW's, and spatial hole burning due to the finite time it takes for the carriers contributing to the lasing to be supplied [7]–[9]. Such effects reduce the differential gain, increase gain compression, and create a single-pole rolloff in the modulation response. There are various approaches to model the carrier dynamics to different degrees of sophistication. The general conclusion is very nonuniform distribution of carriers in the active region and different degrees of carrier modulation in different parts. Typically, the best results are obtained by making the transport time as short as possible, while making the escape time from the well as large as possible [2]. Therefore, narrow SCH widths should be combined with deep multiple QW's (MQW's). Using MQW's also helps to increase both optical and carrier confinement.

In addition to optimizing the material and cavity design for the active layers, extrinsic parasitics should also be minimized. These are device resistance and capacitance as well as the bond-wire inductance. Device resistance components are contact resistance, resistances of doped layers, and resistance associated with heterobarriers. Device capacitance depends on the active region and bondpad areas. Bonding inductance is usually minimized using short ribbons. Most high-speed devices reported in literature are directly probed using coplanar probes, eliminating the effect of the bondwire and other package related parasitics. Furthermore, since bias currents significantly above threshold are used, heat dissipation is high. Therefore, effective heat sinking is very important for high-speed operation. Many intrinsical very high-speed devices had bandwidths limited by heating.

Recently, a device designed using the above principles was reported to have record bandwidth [4]. This device has four 5.7-nm-wide $In_{0.35}Ga_{0.65}As$ QW's separated by 20.1-nm undoped GaAs barriers. This creates deep QW's, which provides strong confinement and suppresses the carrier escape. Undoped GaAs confinement layers on both sides of the MQW region are only 400-A thick. These layers are thin enough to minimize carrier-transport-related problems. The upper and lower cladding layers are $Al_{0.8}Ga_{0.2}As$, creating strong optical confinement. The quality of the material was improved significantly over previous designs, with $I_{\rm th}$ and η_i reported as 8 mA and 70%, respectively. The devices were short-ridge waveguide lasers operating at 1.1 μm. Small-signal CW modulation response of a 6×130 μm^2 device at different bias currents is shown in Fig. 1. As expected, f_r increases with I. At low I, bandwidth is limited by f_r. As I and f_r increase, damping starts to limit the bandwidth. Fig. 2 shows the small-signal modulation response of the same device biased at $I = 155$ mA. The 3-dB modulation bandwidth exceeds 40 GHz and is limited by the damping. These devices have been used for large-signal digital modulation at 20 Gb/s [4].

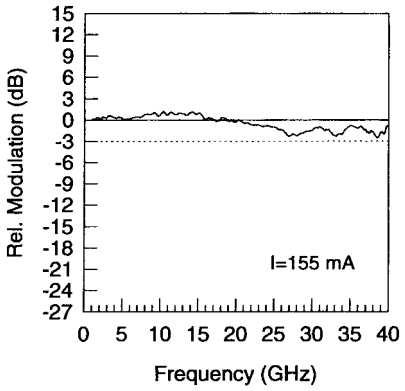

Fig. 2. Small-signal CW modulation response of a 6×130 μm^2 ridge waveguide laser at a bias current of 155 mA [4, Fig. 2]. ©1994 IEEE.

For RF photonic link applications, operation around 1.3 or 1.55 μm may be more desirable due to the more mature technology of other link components such as photodetectors. Operation at these wavelengths requires InGaAsP as the active layer. For such lasers, 3-dB bandwidths as high as 25 GHz have been obtained with buried ridge devices [10], [11]. Ridges were buried in Fe-doped semiinsulating InP. Intrinsic bandwidths were close to 40 GHz, showing that bandwidth was limited by device parasitics.

Another very important concern for link design is the relative intensity noise (RIN) of the laser. RIN directly affects the noise figure of the link and, at the current time, limits the noise figure of most links using semiconductor lasers [1]. The typical RIN spectrum of a semiconductor laser resembles its frequency response [3] peaking at f_r and leveling off on either side. Since the response is limited at frequencies higher than f_r and noise is enhanced close to f_r, the low-noise frequency range is less than its bandwidth. Improvements in f_r reduce RIN and increase the frequency range over which laser can be used. Typical RIN values of high-speed lasers are in the 125–150-dB/Hz range. Distributed feedback (DFB) devices have lower RIN values than Fabry–Perot devices. Signal-to-noise ratio (SNR) at the output of a link, which is limited by the intensity noise of the laser, can be expressed as $\mathrm{SNR} = m^2/(2 \cdot \mathrm{RIN} \cdot \mathrm{BW})$, where BW is the system bandwidth, and m is the modulation index [3]. m values are typically limited by the linearity requirements to a few percent. Typical slope efficiency or external differential quantum efficiency of high-speed lasers is in the 0.1–0.3 W/A range. A significant limitation to slope efficiency is the coupling loss between the laser chip and single-mode fiber.

At the current time, an active research area is exploring the use of p-doped strained QW lasers for enhanced modulation bandwidths. Another emerging research direction is to try to improve the slope efficiency. It is possible to make semiconductor lasers with external differential efficiencies larger than unity by connecting several active regions in series [12], [13]. This can also be done monolithically using a single optical waveguide. This results in the multiplication of the external efficiency by the number of active regions and a reduction of the threshold current of the same number. At biases well above threshold, the RIN should also be

significantly reduced. Furthermore, series connected lasers have larger input impedances and offer better impedance matching to RF sources.

III. Modulators

The most commonly used materials for external modulators are $LiNbO_3$, III–V compound semiconductors, and electrooptic polymers. Of these $LiNbO_3$ and III–V compound semiconductors offer mature material technology and most of the effort is on engineering the optical and microwave characteristics of the device. Polymers offer significant potential, but material technology is still undergoing development. At the current time, there is a significant amount of research effort to develop high-performance electrooptic polymers.

In this section, first electroabsorption (EA) modulators as a lumped circuit components are described. Next, traveling-wave modulators in $LiNbO_3$, GaAs, and electrooptic polymers are discussed. A short section on traveling-wave EA (TW-EA) modulators is also included at the end of this section. The entire treatment is from a device point-of-view. Description of each type of device starts with a short tutorial section. The basic device structure is then introduced and material and fabrication related issues are discussed. This is followed by the discussion of the device and material design issues that determine the key modulator parameters such as drive voltage, bandwidth, optical power-handling capability, bias stability, and insertion loss. Tradeoffs between these important modulator parameters are also discussed. Most recent developments in each area together with emerging research directions are also presented.

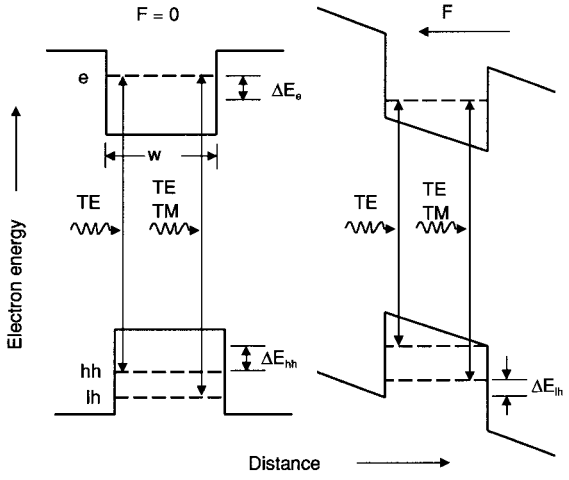

Fig. 3. Schematic of an unstrained QW energy diagram with and without an applied electric field F. e, hh, and lh designate energy levels for electrons, hh's, and lh's, respectively.

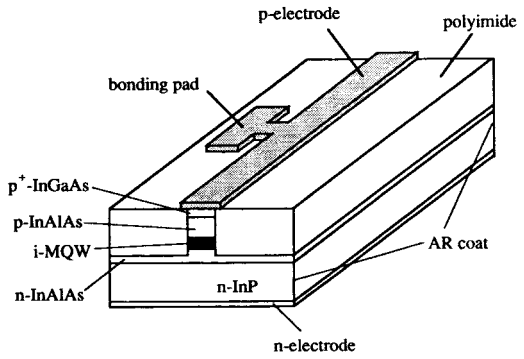

Fig. 4. Schematic of a MQW EA modulator [16, Fig. 1]. ©1994 IEEE.

A. Lumped EA Modulators

QW's in III–V compound semiconductors have many novel properties that led to significant enhancements in optoelectronic devices. One of the most significant effects is the quantum confined Stark effect (QCSE) [14]. In a QW, electrons and holes are confined in the same physical QW. As a result, they overlap and interact strongly and form a bond similar to a hydrogen atom. This is called an exciton and has a strong absorption somewhat similar to an atomic absorption. Spectra of such strong excitonic absorption is very sharp, and is localized in the vicinity of wavelengths corresponding to the bandgap of the QW. When an external electric field is applied, electron and hole are forced to opposite ends of the QW and are physically separated. These arguments are illustrated in Fig. 3. As a result, the spatial overlap or interaction of the electron and the hole is reduced and excitonic absorption is decreased and broadened. This makes it possible to modulate the absorption very strongly with external fields around a narrow wavelength range and is known as the QCSE. If such QW's are embedded in an optical waveguide, the insertion loss of this waveguide can be modulated by applying an electric field and changing the absorption of the QW's through the QCSE [15]. Fig. 4 shows such a modulator [16]. Typically, MQW's are used to increase absorption and are embedded in the i region of a reverse biased p-i-n diode. The typical thickness of the i region, d_i, is in the 0.1–0.5-μm range. Therefore, it is possible to apply very strong electric fields with a few volts of reverse bias. In this case, well and barrier material are InGaAs and InAlAs, respectively. The index of refraction of the top p and bottom n-InAlAs is lower than that of MQW. This forms a slab waveguide. By deeply etching this slab waveguide, a channel optical guide is formed. Waveguide widths are at the order of 1–3 μm and the etch depths are about 1–2 μm. Typical device lengths are in the 50–300-μm range. Ohmic contacts are formed at the top and bottom. Etched areas underneath the bonding pads are filled with a low dielectric constant polyimide to reduce device capacitance. Since only the absorption modulation is utilized, the optical waveguide need not be single mode. Therefore, the profile of the optical waveguide can be optimized for improved coupling to the incoming fiber mode. However, critical control of the composition and thickness of the epitaxial layers are required.

Fig. 5 shows the photocurrent spectra of an unstrained MQW material as a function of wavelength at different applied voltages [16], [17], where device photocurrent is proportional to optical absorption. Two peaks are resolved in the absorption spectra. These are due to excitons formed between electrons and hh's and electrons and lh's. Transition energies of hh and lh excitons are different due to different effective mass of lh's and hh's, as seen in Fig. 3. Furthermore, the excitons interact with different optical polarizations. The hh excitons interact

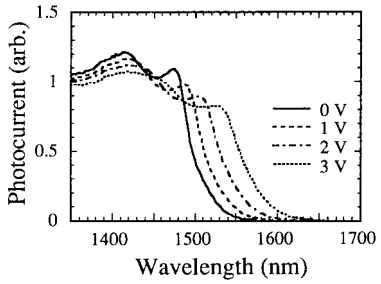

Fig. 5. Photocurrent spectra of an unstrained MQW modulator as a function of bias voltage. The incident light is TE polarized [16, Fig. 2]. ©1994 IEEE.

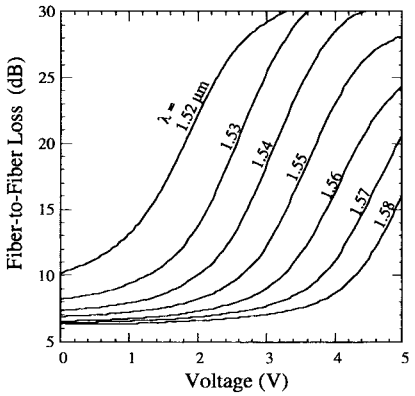

Fig. 6. Fiber-to-fiber insertion loss of a 40-Gb/s EA modulator for various wavelengths. The input light was TE polarized [22, Fig. 10]. ©1996 IEEE.

with TE polarized light and lh excitons interact with both TE and TM polarized light. In Fig. 5, the first absorption peak has a lower transition energy or higher optical wavelength and corresponds to the lowest hh exciton indicated in Fig. 3. The second absorption peak corresponds to the lh exciton. As bias voltage increases, absorption characteristics broaden and peak absorption decreases and moves toward longer wavelengths. For example, at 1.55-μm absorption is modulated strongly when bias changes between 0 and 3 V. This makes it possible to make a very simple modulator, which is a very short waveguide.

The transmission through such a modulator as a function of applied voltage can be expressed as

$$T(V) = K \exp\Big[-\Gamma \alpha(V) l\Big] \tag{5}$$

where Γ is the overlap between the optical mode and the MQW, $\alpha(V)$ is the absorption coefficient as a function of applied voltage V, l is the length, and K is the coupling coefficient between the fiber and optical waveguide. The on/off ratio of an EA modulator in decibels can be expressed as

$$\begin{aligned} 10\log\left[\frac{T(V)}{T(0)}\right] &= \frac{\alpha(V)-\alpha(0)}{\alpha(0)} 10\log\Big[e^{-\alpha(0)L}\Big] \\ &= \frac{\Delta\alpha}{\alpha}[\text{Propagation loss (dB)}]. \end{aligned} \tag{6}$$

Optical propagation loss of EA modulators is large, typically in the 15–20-dB/mm range. Main components of this loss are the free carrier absorption, especially in the p layers, and band-to-band absorption. The second loss component can be made smaller by increasing the separation between the wavelength of operation and the absorption peak, which is called detuning. Typical detuning values are about 20–50 nm. Typical $\Delta\alpha/\alpha$ values are in the 3–10 range. Large on/off ratio devices can be obtained using long devices, but that also increases the insertion loss. For the typical EA modulator lengths in 50–300-μm range propagation loss is 1–3 dB. Therefore, to get large extinction ratios with low device insertion loss, $\Delta\alpha/\alpha$ should be maximized. Furthermore, efficient modulation requires a large $\Delta\alpha/\Delta V$ or $(1/d_i)(\Delta\alpha/\Delta F)$, where F is the applied electric field. In other words, large Stark shifts are required. For low-bias voltages, the shift in the ground state energy ΔE_i of a particle in a QW can be approximated as [18]

$$\Delta E_i = D m_i w^4 F^2, \qquad i = e, \text{hh}, \text{lh} \tag{7}$$

where m_i is the effective mass of the particle, w is the width of the QW, and D is a constant. Hence, wide QW's are desired for efficient operation. These energy shifts are shown in Fig. 3.

For fiber-optic communication applications, the desired wavelength is around 1.55 μm. This requires alloys of InP and GaAs as active material grown on InP substrates. Quaternary alloys such as InGaAsP and InGaAlAs can be grown lattice matched to InP and make it possible to change the bandgap energy and well thickness independently [19], [20]. Thick QW's up to 12 nm have been reported in InGaAsP/ InGaAsP MQW, resulting in drive voltages as low as 1.2 V [19]. Similarly, InGaAlAs/InAlAs MQW's with well widths as large as 19.6 nm yielded very low voltage EA modulators at 1.55 μm, requiring about 1 V for 10-dB on/off ratio [21]. Larger electron confinement due to increased conduction band discontinuity in this material system makes such wells comparable to narrower wells in the InGaAsP system. It is possible to obtain similar results using lattice-matched InGaAs ternary QW's. However, as the wells get thicker, the absorption edge shifts to longer wavelengths and operation around 1.55 μm becomes difficult. This difficulty in the ternary material can be eliminated by using a tensile-strained QW [17]. A commonly used material design consists of an 0.6-μm n-InAlAs buffer, an undoped strained MQW absorption layer, a 2-μm p-InAlAs cladding layer, and a p^+-InGaAs contact layer [22]. The strained MQW layer contains ten 8.8-nm $In_{0.48}Ga_{0.52}As$ wells and 5-nm $In_{0.53}Al_{0.47}As$ barriers. The wells are under 0.35% tensile strain and the barriers are under 0.5% compressive strain. The strain in the barriers is used for strain compensation. Proper amounts of alternating compressive and tensile strain can make the total strain in the MQW near zero, allowing large periods of strained MQW without exceeding the critical layer thickness. Fiber-to-fiber insertion loss of a typical high-speed EA modulator as a function of external bias at different wavelengths is shown in Fig. 6 [22]. QCSE is most pronounced for photon energies near the bandgap of the material and shows a strong wavelength dependence, as seen in Fig. 6. At shorter wavelengths, modulation becomes more efficient, but insertion loss also increases.

For RF photonic applications, another desirable wavelength is 1.3 μm. This wavelength is in the low-loss window of the

standard single-mode fiber and coincides with its dispersion minimum. Furthermore, high-power low-RIN single-frequency solid-state lasers are commercially available around 1.3 μm. This is a very important consideration for RF photonic links because, as shown earlier, high optical powers result in high link gains. 1.3-μm EA modulators have been realized both on InP and GaAs substrates. On InP, lattice-matched quaternary alloys can provide operation at 1.3 μm. It is also possible to use strained wells and barriers. In one approach, a MQW containing 11 periods of 9.5-nm-thick compressively strained $InAs_{0.41}P_{0.59}$ QW's and 13.5-nm-thick tensile-strained $Ga_{0.13}In_{0.87}P$ barriers were imbedded in the i region of a p-i-n modulator on an n^+ InP substrate [23]. MQW is positioned between p and n doped passive $In_{0.87}Ga_{0.13}As_{0.29}P_{0.71}$ waveguiding layers. Fiber-to-fiber insertion loss of a 220-μm device was quoted to be 9 dB. dc bias required for 15-dB on/off ratio was slightly over 3 V.

It is also possible to fabricate 1.3-μm EA modulators on GaAs substrates. GaAs substrates offer potential for monolithic integration with GaAs monolithic microwave integrated circuits (MIMIC's). However, this presents a challenge because of lattice mismatches as large as 2.5% between the active layers and GaAs substrate. Lattice mismatch issue is typically addressed by growing compositionally graded $In_xAl_{1-x}As$ relaxed buffer layers [24]–[27]. It was possible to grow ten periods of 9.5-nm-wide $In_{0.36}Ga_{0.62}As$ wells with 10-nm-thick $In_{0.36}Al_{0.64}As$ barriers using only a 0.7-μm-thick three-stage compositionally step graded $In_xAl_{1-x}As$ buffer layer [27]. The MQW stack is sandwiched between 0.5-μm-thick p- and n-doped $In_{0.36}Ga_{0.32}Al_{0.32}As$ waveguide layers with a bandgap energy of 1.1 μm. In this design, the total thickness of the $In_xAl_{1-x}As$ buffer layer is important since its index is smaller than the waveguiding layers and GaAs substrate and, for thinner buffer layers, significant leakage to the substrate can result.

EA modulators are very short devices and, hence, have small device capacitance. Therefore, when driven as a lumped-circuit element, their speed of operation will be limited by the *RC* time constant of the circuit. Therefore, reducing the capacitance by shortening the device increases the speed of operation. Typically, a 2.5-μm-wide and 150-μm-long device has a capacitance of about 0.33 pF, which is low enough for 20-GHz bandwidth when driven by a 50-Ω source with a 50-Ω terminating resistance across the device. Higher bandwidths are possible by using a lower terminating resistance. This reduces the *RC* time constant; hence, increases the bandwidth at the expense of modulation efficiency. Electrical 3-dB bandwidths approaching 60 GHz have been reported for lumped devices [22], [28]–[30]. High-speed operation requires not only a short device, but also good impedance matching and proper microwave packaging. Although unpackaged devices demonstrated very high-speed operation, it was difficult to duplicate these results in packaged modules. The main source of the difficulty is cleaving and packaging devices as short as 50 μm. One solution to this difficulty is to integrate passive input and output waveguides to a very short EA section [22]. This requires etching of the MQW region outside the EA modulator section and regrowing low-loss passive waveguide

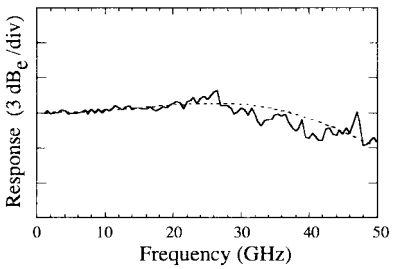

Fig. 7. Frequency response of an EA modulator with integrated input and output optical waveguides under 1.5-V reverse bias and +5-dBm optical input power at 1.55 μm. The dashed line shows the calculated data [22, Fig. 11]. ©1996 IEEE.

sections. This technique was used to obtain overall device lengths of 1 mm, with EA modulator sections as short as 50 μm. The measured frequency response of such a 1.55-μm modulator is shown in Fig. 7, showing a 3-dB electrical bandwidth of 50 GHz. At 1.3 μm, bandwidths as large as 38 GHz have been demonstrated [31].

Optical power-handling capability of EA modulators has also been investigated. For large optical power-handling, photogenerated carriers should escape from the QW's and should be easily collected by the ohmic contacts. Escape and collection is typically a problem for the hh's due to their larger effective mass, which makes it more difficult for them to tunnel out of the QW. The resultant carrier pile up screens the electric field inside the QW. The decreased field further inhibits the carrier escape and enhances carrier pile up. The end effect is the saturation of the absorption and degradation in the modulation response [32]. Therefore, material designs with lower hh mass and valence band discontinuity are highly desirable. Tensile strain in QW helps to achieve this. Tensile strain reduces the hh mass and barrier heights for electrons and hh's [33]. At the same time, barrier height for lh's slightly increases [33], [34]. This results in the reduction of photogenerated carrier sweep out times decreasing the carrier pile up in the wells. Therefore, optical saturation performance of the EA modulator improves. Carrier escape times of strained and unstrained EA modulators were measured from the modulator photo response to a short optical pulse with large peak powers [35]. Increase in the decay time with increasing peak optical power was found to be significantly larger for the modulator with lattice matched MQW. Increasing the bias field restores decay time; however, this cannot be done indefinitely because it would eventually bias the modulator to the off state. No degradation was observed in the frequency response of strained modulators up to coupled input powers of 3 mW. In the unstrained material, there was a definite degradation at low bias values. 1.3-μm devices on InP substrates described earlier were used in RF links and link efficiency as high as -38 dB was realized [23]. RF link efficiency was found to linearly increase with the optical power up to 10 mW, which was the limit of the available optical power. At this optical power, no degradation in the speed of operation was observed [23]. High-power operation of bulk EA modulators up to 34 mW without degradation in the speed has also been reported [36]. At high optical powers, power dissipation in the device

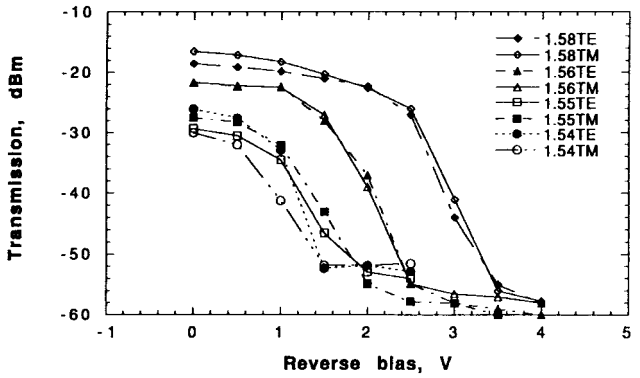

Fig. 8. Optical transmission characteristics of a strained MWQ modulator for both TE and TM polarizations at wavelengths of 1.54, 1.55, 1.56 and 1.58 μm [38, Fig. 2]. ©1995 IEEE.

increases due to increased photocurrent. The resultant thermal heating decreases the bandgap. Bandgap shrinkage increases absorption, hence, the slope efficiency of the device [37]. However, increased slope efficiency at optical power levels exceeding 50 mW was not observed in RF measurements and shown to be a low-frequency effect [37]. Therefore, proper heat sinking is essential at high optical powers.

Another significant benefit of strain compensated QW's is the polarization independence of the EA [17], [38], [39]. Strain affects the hh and lh transition energies differently due to different valence band offsets under strain. The most common approach is to use about 0.5% tensile-strained InGaAs wells and about 0.5% compressive-strained InAlAs barriers [38], [22]. Tensile strain brings the valance band closer to the conduction band and lifts the degeneracy between the heavy and lh bands at the zone center. The shift in the lh band is more than that in the hh band. This compensates for the larger quantum confinement energy of the lh's and transition energies for the hh's and lh's can be made identical. Optical transmission of such a device is shown in Fig. 8 [38]. This approach achieves degeneracy between hh and lh excitons at zero and low biases. As the bias field increases, absorption for TE and TM polarizations start to differ due to different effective mass of hh's and lh's. Equation (7) shows that the Stark shift for hh's, which interact with TE polarized light only, is larger due to heavier effective mass. As a result, absorption change for TE polarization is more than TM polarization as applied electric field increases. A recently proposed scheme addresses this problem by creating different effective QW widths for hh's and lh's [40]. This is achieved by introducing thin barriers in the QW. If the thickness of these thin barriers is appropriate, lh's can tunnel through them and are confined by the original QW. Therefore, the effective quantum confinement width they experience is mainly determined by the width of the QW. However, the hh cannot tunnel through the barriers and experience a quantum confinement width determined by the distance between the thin barriers in the QW. As a result, effective QW width for lh's is larger than the effective QW width for the hh's. By engineering this modified QW, it is possible to make the mL^4 term the same for both hh's and lh's. The Stark shifts for both hh's and lh's will then be identical at all fields. Transition energies and absorption strengths can also be made the same by tensile straining the whole well. Polarization-independent modulators based on this principle were demonstrated using GaAs wells and $In_x(Al_yGa_{1-y})_{1-x}As$ barriers on GaAs substrates over 28-nm range around 870 nm [41].

EA modulator characteristics are very sensitive to wavelength and temperature changes, as seen in Fig. 6. Therefore, bias control is needed during operation. This can be achieved by monitoring part of the output and using a feedback loop, which requires a dedicated photodetector. However, the EA modulator also works as a photodetector and this detected current can be used to monitor the bias-point variations. Recently, it was shown that the bias where the slope of the dc photo current is largest coincides with the bias point that achieves the maximum RF link gain [42]. This is because RF link gain is proportional to the square of the modulator slope efficiency, and modulator photocurrent is a measure of the modulator transmission as long as the modulator is not saturated. Therefore, tracking the dc photo current of the modulator and keeping its bias sensitivity maximum keeps the RF link gain maximum [42]. This was found to be the case for different input polarizations, wavelengths and power levels. However, when the input optical power level approaches the modulator saturation level, this approach is no longer applicable.

One can also take advantage of wavelength sensitivity of the modulator transfer function for broad-band linearization. The idea is to apply two optical carriers at different wavelengths and power levels to the same modulator while applying a single dc bias and RF signal [43]. Both optical carriers are modulated at different levels since they are at different wavelengths. If one of the wavelengths is chosen as the operation wavelength, it is possible to adjust the amplitude and wavelength of the other carrier such that modulation sidebands at the desired harmonic can be canceled when both optical carriers are detected using the same high-speed photodetector [43]. Using this approach, 30-dB reduction at the third-order harmonic distortion was achieved at fundamental microwave frequency as high as 10 GHz.

Currently, device research on EA modulators is on reducing the drive voltage, while increasing the on/off ratio and the bandwidth. This presents conflicting requirements because, for lumped operation, wide bandwidth requires a short device, whereas for a short device, on/off ratio is low and operation voltage is high. In one approach, a double-pass modulator was proposed and demonstrated [44]. This is achieved by antireflection coating the front facet and high-reflection coating the back facet and making the light pass through the device twice. Therefore, device capacitance remains unchanged, but absorption length is doubled. Experimentally drive voltage reduction of about 60% was realized using an InGaAsP bulk EA layer [44]. Another recent research direction is to use the EA modulator as a traveling-wave device, which is described in Section III-D.

B. Traveling-Wave Modulators

A very well-established approach to obtain very wide-bandwidth modulators is the so-called traveling-wave design

[45]–[48]. In such a design, the electrode is designed as a transmission line. Therefore, electrode capacitance is distributed and does not limit the modulator speed due to *RC* time-constant limitations. The modulating electrical signal on the electrode travels in the same direction as the modulated optical signal. If they travel with the same velocity, the phase change induced by the electrical signal is integrated along the length of the electrode. Since the electrode capacitance is not the bandwidth limit, one can make the electrode very long, typically thousands of wavelengths. This allows even a very small phase change over a wavelength to accumulate to an appreciable value. Therefore, drive voltage requirements can be significantly relaxed without sacrificing electrical bandwidth. In such designs, the properties of the electrode determine the main properties of the modulator such as bandwidth and drive voltage. Obviously, this approach will be most efficient if the group velocities of the electrical and optical signals are matched [77], [79], [80]. In addition to group velocity matching, characteristic impedance of the electrode should be matched to that of the driver. This impedance value is almost universally 50 Ω. If the termination is different than the characteristic impedance, a standing-wave pattern will be generated on the electrode. This pattern will be frequency dependent; hence, the effective voltage on the electrode will change as a function of frequency. This, in turn, changes the modulation efficiency and creates ripples on the modulation response as a function of frequency [49]. The most notable of these effects is a sudden decrease in the modulation efficiency at low microwave frequencies. A standing wave consists of forward and backward traveling waves. At very low frequencies, both waves contribute to the modulation. However, as frequency increases, the backward wave becomes velocity mismatched and part of the voltage associated with it does not contribute to the modulation reducing efficiency. One can eliminate the standing-wave effects by terminating the electrode with a load having the same impedance as the characteristic impedance of the electrode. However, in this case, microwave drive power requirements will be increased and some of the available power from the source will be lost due to reflections originating from the impedance mismatch between the driver and electrode. Since almost all microwave sources have 50-Ω output impedance, it is imperative that the modulator electrode characteristic impedance is as closely matched to 50 Ω as possible. The small-signal modulation response of a traveling-wave modulator with a characteristic impedance matched to both the driver and load impedance is given as [50]

$$M(f) = e^{-\left(\frac{\alpha l}{2}\right)} \left[\frac{\sinh^2\left(\frac{\alpha l}{2}\right) + \sin^2\left(\frac{\xi l}{2}\right)}{\left(\frac{\alpha l}{2}\right)^2 + \left(\frac{\xi l}{2}\right)^2} \right]^{\frac{1}{2}} \tag{8}$$

where

$$\xi = (n_\mu - n_o)\frac{2\pi f}{c}. \tag{9}$$

α and l are the loss coefficient and length of the electrode, respectively, f is the RF drive frequency, c is the speed of light in vacuum, and n_μ and n_o are the microwave and optical indexes. Based on (8), if there is no velocity mismatch, the 3-dB bandwidth will be at the frequency where the total electrode loss becomes 6.34 dB. Therefore, a low-loss velocity- and impedance-matched electrode is essential for the realization of a very wide-bandwidth traveling-wave modulator. Finally, another crucial requirement for the electrode is to generate a strong electric field overlapping very well with the optical mode and directed in a certain direction dictated by the electrooptic material. This is important to reduce the drive voltage of the modulator. All these requirements on the electrode are often conflicting, and compromises are required. Furthermore, depending on the material used, the properties of the electrode, most notably the microwave velocity, could be very different. In the following sections, traveling-wave modulator designs in different material systems are described.

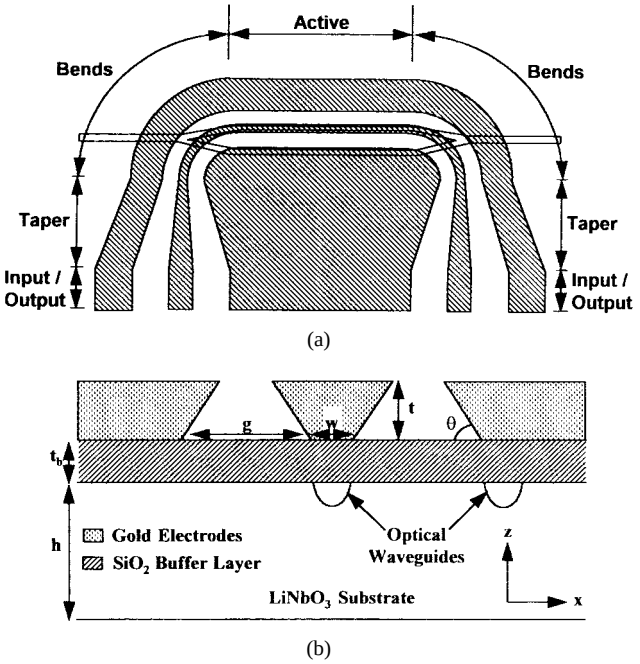

Fig. 9. (a) Top view and (b) cross-sectional schematics of a z-cut y-propagating $LiNbO_3$ traveling-wave modulator [49, Fig. 1]. ©1994 IEEE.

1) $LiNbO_3$ Traveling-Wave Modulators: Among all external modulators, $LiNbO_3$ traveling-wave modulators have the most mature technology. Such modulators are commercially available from several manufacturers and are used in commercial applications. $LiNbO_3$ is a ferroelectric crystal that is commonly used in other types of commercial products, most notably, in surface acoustic-wave filters for mobile communication receivers. The large market for such components is the driving force that makes $LiNbO_3$ crystals readily available.

A schematic of a typical $LiNbO_3$ traveling-wave modulator is shown in Fig. 9 [49]. The optical structure is a Mach–Zehnder interferometer. The most common way of fabricating optical waveguides in $LiNbO_3$ is Ti indiffusion. Typically, Ti stripes from about 3- to 8-μm-wide and about 0.1-μm thick are patterned on the surface of $LiNbO_3$ using liftoff. These Ti stripes are subsequently driven into $LiNbO_3$ around 1000 °C for about 10 h in an oxygen atmosphere. The resulting Ti diffusion profile translates itself into a higher

index of refraction and optical guiding results. The index steps generated this way are on the order of 0.01, and typical optical propagation loss coefficients are less than 0.2 dB/cm. Furthermore, the optical modes in such waveguides match rather well with the mode of a single-mode optical fiber. As a result, 5-dB fiber-to-fiber insertion is quite common for $LiNbO_3$ traveling-wave modulators with 5-cm-long electrodes. Other techniques of fabricating optical waveguides in $LiNbO_3$ include ion exchange, proton exchange, and Ni diffusion.

$LiNbO_3$ is an anistropic crystal with 3-m crystal symmetry. Depending on the orientation of the applied electric field, different electrooptic coefficients are possible [51]. The most commonly used coefficient is the r_{33}, which is the largest diagonal coefficient. Its value is about 30 pm/V. For x-cut y-propagating crystals, a horizontal electric field parallel to the surface of the crystal, i.e., an electric field along the z-axis, is utilized. This configuration modulates the TE polarized optical mode, in which the main electric-field component of the optical waveguide mode is parallel to the surface of the crystal, i.e., it is along the z-axis of the crystal. For z-cut crystals, an electric field vertical to the surface of the crystal is used. Optical waveguides are along the y-axis of the crystal, as shown in Fig. 9. This field modulates the TM polarized optical mode most efficiently. For TM modes, the main electric-field component of the optical waveguide mode is also perpendicular to the surface of the crystal, i.e., it is along the z-axis of the crystal. For both configurations, the modulating external field and main electric-field component of the optical mode are parallel to each other and to the z-axis of the crystal. The resulting index change is

$$\Delta n = \pm \frac{1}{2} n^3 r_{33} F_z \tag{10}$$

where n is the optical index of refraction and F_z is the component of the applied electric field along the z-axis. The dielectric constant of $LiNbO_3$ shows a large amount of dispersion going from microwave to optical frequencies due to large ionic contribution to its dielectric constant. For z-cut crystals, the microwave relative dielectric constants of $LiNbO_3$ parallel and perpendicular to the crystal are $\varepsilon_{ry} = 43$ and $\varepsilon_{rz} = 28$, respectively. For a transmission line running along the y-direction, one can define an effective relative dielectric constant under quasi-static approximation as [52]

$$\varepsilon_{\text{reff}} = \sqrt{\varepsilon_{ry}\varepsilon_{rz}} \tag{11}$$

which is around 35. The most commonly used electrode for such modulators is the coplanar waveguide (CPW). The effective microwave index of a CPW on $LiNbO_3$ with zero conductor thickness and top dielectric as air is [53]

$$n_\mu = \sqrt{\frac{\varepsilon_{\text{reff}} + 1}{2}} = \sqrt{\frac{\sqrt{\varepsilon_{ry}\varepsilon_{rz}} + 1}{2}}. \tag{12}$$

This value is larger than four. On the other hand, the commonly assumed effective index of an optical mode in a Ti indiffused $LiNbO_3$ optical waveguide is 2.15. As a result, an electrical signal applied to the electrode will travel significantly slower than the optical wave. Therefore, velocity matching in $LiNbO_3$ modulators requires increasing the velocity of propagation of the microwave electrode.

The most common way of achieving this is to use a SiO_2 buffer layer under the electrode and to increase the thickness of the conductors. The characteristic impedance Z_0 and the velocity of propagation v_μ of a transmission line are given as

$$Z_0 = \sqrt{\frac{L}{C}} \quad v_\mu = \frac{1}{\sqrt{LC}} \tag{13}$$

where L and C are the inductance and capacitance per unit length of the transmission line, respectively. Under quasi-static approximation, L is found using the same exact line geometry in which the dielectrics are replaced by air. Since electrooptic materials used are nonmagnetic, L of this air line is the same as the L of the original line. However, the capacitance per unit length of the air line C_a is different. Such a line with uniform air dielectric supports a TEM mode with velocity of propagation the same as the speed of light in air c. Hence,

$$c = \frac{1}{\sqrt{LC_a}} \quad \text{or} \quad L = \frac{1}{c^2 C_a}. \tag{14}$$

Combining these equations together, we find that

$$v_\mu = c\sqrt{\frac{C_a}{C}} \quad \text{and} \quad Z_0 = \frac{1}{c\sqrt{CC_a}}. \tag{15}$$

Relative dielectric constant of SiO_2 is 3.9, which allows filling part of the transmission line with a low index medium. This, in turn, reduces C, hence, v_μ and Z_0 are increased. Placing a dielectric-like SiO_2 under the metal electrode also helps to reduce the overlap of the optical mode with the metal electrode. This helps to reduce the optical propagation loss significantly, especially for z-cut devices. However, thick SiO_2 layers are not desirable since part of the electrode voltage that drops across this layer reduces the electric-field intensity in $LiNbO_3$; hence, modulation efficiency of the device. Typical SiO_2 layer thickness is about 1 μm. The additional velocity increase is typically achieved by increasing the conductor thickness. Increasing the conductor thickness increases the electric-field strength in the slots between the conductors. This, in turn, increases C_a; hence, v_μ increases and Z_0 decreases. Typical conductor thicknesses range from 10 to 20 μm. For such thick electrodes, the slope of the sidewalls start to effect the electrode characteristics [49]. Although it is possible to achieve velocity matching this way, the undesirable side effect is the reduction in the characteristic impedance of the electrode. It is possible to adjust the gap and width of the center conductor of the CPW to match v_μ and Z_0 simultaneously, but this requires rather narrow gap and width values [54]. As a result, microwave electrode loss increases and becomes the limiting factor for the bandwidth. This difficulty was solved by introducing the ridge structure [55].

Fig. 10 illustrates the basic idea behind this approach [55]. Compared to the conventional modulator, the ridge removes the high microwave dielectric constant $LiNbO_3$ between the conductors. As a result, C reduces and both v_μ and Z_0 are increased simultaneously. This allows velocity matching without sacrificing impedance matching. Furthermore, a high

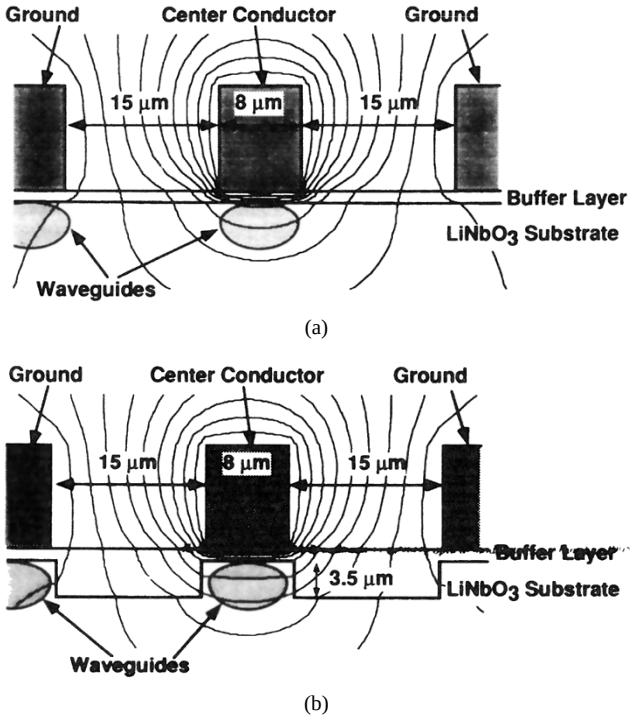

Fig. 10. Cross-sectional schematic and potential distribution around the center conductor of: (a) conventional modulator and (b) ridge structure [55, Fig. 3]. ©1993 IEEE.

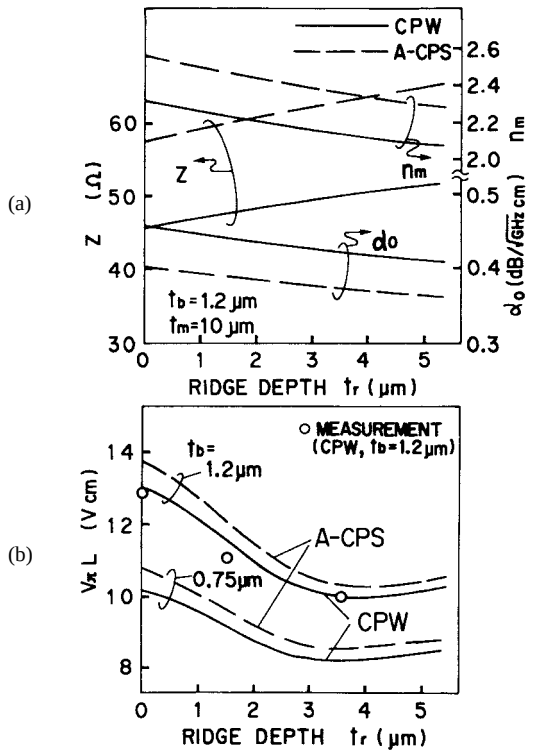

Fig. 11. Calculated results of: (a) microwave effective index n_m, characteristic impedance, Z_0, and conductor loss at 1 GHz, α_0. (b) Drive voltage length product $V_\pi \cdot L$ of an $LiNbO_3$ traveling-wave modulator with ridge structure as a function of ridge depth t_r for CPW and A-CPS electrodes [56, Fig. 2]. ©1995 IEEE.

dielectric constant in the ridge helps to confine the electric-field lines under the electrode such that field becomes almost vertical under the electrode. As a result, the desired vertical component of the electric field overlaps better with the optical mode, improving the efficiency of the modulator. This is especially true for the z-cut devices.

Detailed analysis of this modulator geometry was reported in [56]. Microwave characteristics of the electrode were calculated using a quasi-static analysis based on the finite-element method. Both a CPW and an asymmetrical coplanar strip line (A-CPS) were considered in the calculations. The center conductor width W and the gap G between the electrodes for both transmission lines were 8 and 15 μm, respectively. The electrode loss is assumed to be entirely due to conductor losses. Conductor losses are assumed to depend on frequency as

$$\alpha(f) = \alpha_0 \sqrt{f} \tag{16}$$

where α_0 is the conductor loss at 1 GHz. α_0 was calculated using the incremental inductance formula [53]. The drive voltage V_π of the modulator was calculated using numerically obtained overlap integral between the vertical electric-field component and optical mode. Fig. 11 shows the effect of ridge thickness t_r on the microwave characteristics and drive voltage of the modulator for a buffer-layer thickness $t_b = 1.2$ μm and electrode thickness of $t_m = 10$ μm. As expected, microwave index and α_0 monotonically decrease when t_r increases. At the same time Z_0 monotonically increases. As described earlier, this is due to a monotonic decrease in C as t_r increases. V_π initially decreases and then saturates at t_r of about 3–4 μm. The calculated values for the CPW electrode agree rather well with the experimental data reported in [57].

Assuming the optimum t_r value as 3 μm, V_π and microwave characteristics of the modulator were calculated for different t_b and t_m values. Results shown in Fig. 12 indicate that v_μ, Z_0, and α_0 of the electrode depend strongly on t_b and t_m values. As t_b becomes thicker, v_μ and Z_0 increase and α_0 decreases. V_π only depends on the buffer-layer thickness increasing with t_b, but this increase is less than that of the conventional modulator geometry, mainly due to improved overlap integral. This figure shows that, in a ridge structure, it is possible to get both velocity and impedance match with low conductor loss without significantly sacrificing the drive voltage. For example, for $t_b = 1.0$ μm, $t_r = 3.0$ μm and $t_m = 10$ μm, velocity and impedance match are achieved simultaneously with a low α_0 value of 0.3 dB/GHz$^{1/2}$. An independent analysis indicated that for the same W, G, t_b, and t_m values, the microwave index would be about 2.4 and $Z_0 = 42$ Ω for a conventional modulator design [54]. This corresponds to about 5% velocity mismatch, which can severely limit the bandwidth for long electrodes. In the conventional structure, one can obtain simultaneous impedance and velocity match by changing the CPW geometry. For example, for the thicknesses quoted earlier, $W = 4.3$ μm and $G = 14$ μm would give simultaneous match [54], but the much decreased W would result in an increase in α_0, which again would limit the bandwidth. Fig. 13 shows the optical 3-dB bandwidth and V_π as a function of buffer-layer thickness for an electrode length of 2.7 cm and t_r of 3 μm for different t_m values. The optical 3-dB bandwidth in this figure corresponds an electrical 6-dB

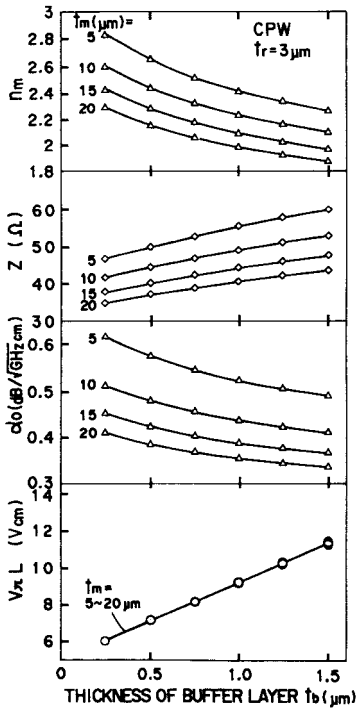

Fig. 12. Microwave effective index n_m, characteristic impedance Z_0, conductor loss at 1 GHz α_0, and drive voltage length product $V_\pi \cdot L$ of an $LiNbO_3$ traveling-wave modulator with ridge structure as a function of buffer-layer thickness t_b for CPW electrodes [56, Fig. 3]. ©1995 IEEE.

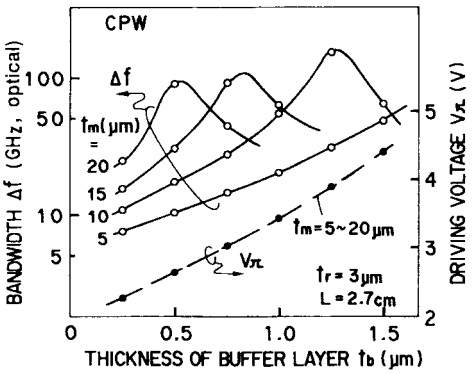

Fig. 13. Optical 3-dB bandwidth and drive voltage V_π as a function of buffer-layer thickness t_b for CPW electrodes for $t_r = 3$ μm and electrode length $L = 2.7$ cm. Optical 3-dB bandwidth is 6-dB electrical bandwidth [56, Fig. 5(a)]. ©1995 IEEE.

bandwidth. Optical bandwidths approaching 100 GHz with V_π values less than 4 V should be possible. Such a modulator with $t_r = 3.4$ μm, $t_b = 1.2$ μm, $t_m = 10$ μm, and $L = 2.0$ cm has demonstrated an optical bandwidth of 75 GHz with a 5-V drive voltage [57]. Under velocity and impedance-matching conditions, the main bandwidth limit is due to electrode loss. One can further reduce the electrode loss by increasing the gap of the CPW [58]. By increasing the electrode thickness, simultaneous velocity and impedance match can be achieved with low electrode loss and without a significant increase in V_π. Frequency dependence of the modulation response of a modulator fabricated using this approach is shown in Fig. 14. For this modulator, $t_b = 1.0$ μm, $t_r = 4.0$ μm, $t_m = 20$ μm, $L = 2$ cm, $W = 8$ μm, and $G = 25$ μm. The measured

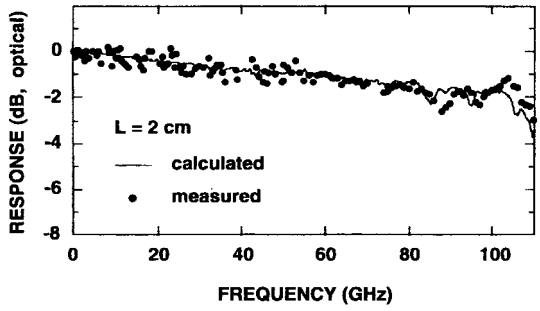

Fig. 14. Modulation response as a function of frequency for a broad-band $LiNbO_3$ traveling-wave modulator employing ridge structure [58, Fig. 9]. ©1998 IEEE.

electrical and optical bandwidths are 75 and 110 GHz, respectively, and V_π is 5.1 V [58]. If the length of the same device is increased to 3 cm, V_π decreases to 3.5 V, but the electrical and optical bandwidths also decrease to 30 and 45 GHz, respectively. Recently, a careful loss measurements up to 110 GHz revealed that up to 20-GHz loss is dominated by conductor losses [59]. Above 20 GHz, dielectric and radiation losses become important. The SiO_2 buffer layer is found to have a loss tangent four times higher than that of the $LiNbO_3$ substrate [59]. Therefore, the quality of this buffer layer needs to be carefully controlled. Another loss component is the coupling to substrate modes in a CPW structure [60]. The usual technique to eliminate this loss is to thin the $LiNbO_3$ substrate. Typical substrate thickness used is less than 0.5 mm. The thinner the substrate, the higher the frequency at which this coupling occurs. Also keeping a large part of the substrate covered with metal helps to eliminate this coupling. CPW electrodes provide an advantage in this regard. In the measurements in [59], several narrow-band electrode loss increases at 85, 95, and 105 GHz were reported. This observation was attributed to coupling to substrate modes in the electrical connectors.

The recent results in the bandwidth of $LiNbO_3$ modulators are impressive. However, drive voltages required to drive such modulators at high frequencies are still high. Present-day electronics is expected to generate about 3.5-V drive voltages at 40 GHz and even less at higher frequencies. That means the drive voltages of existing modulators need to be reduced even further. One obvious way is to increase the electrode length. In a recent work, a reflection type traveling-wave modulator was reported [61]. This approach reflects the electrical and optical signals from the cleaved and polished edge of the substrate. The reflection doubles the interaction length with the electrode. For an electrode and interaction length of 5.3 and 10.6 cm, respectively, V_π was 0.89 V at 1.3 μm.

$LiNbO_3$ is susceptible to what is known as photorefractive effect [62]. Under optical illumination, electrons from ionized impurity centers (typically F^{2+}) are excited to the conduction band. They then move around until they are recaptured by traps. This creates charge separation, which creates large electric fields inside the material. These electric fields change the index through the electrooptic effect. Propagation loss also changes. This is a time-dependent process depending on the charge dynamics and changes in the illumination levels. This

effect is most significant at wavelengths shorter than about 870 nm [63]. It becomes less of an issue at infrared wavelengths like 1.55 μm for typical power levels used in communication applications. It is shown that photorefractive sensitivity of Ti indiffused $LiNbO_3$ modulators can be reduced significantly using high-temperature O_2 anneals [64]. Annealed modulators were operated at 1.3 μm at input optical powers as high as 400 mW up to 168 h with only a 3.5° drift in the modulator bias point. There was no measurable change in the bias point at 100 mW. It is also shown that annealing at high temperatures in N_2 and Ar ambients increases the sensitivity to the photorefractive effect significantly [64].

Bias stability of modern-day $LiNbO_3$ devices is very good. They can operate at constant bias for thousands of hours under the control of automatic biasing circuitry. However, when bias voltages change suddenly, bias drifts with time constants from hours to many days may be observed. The major source of bias-point drift was attributed to flow and redistribution of electrical charge under the application of applied voltages. The conductivity of SiO_2 buffer and $LiNbO_3$ are very high, but finite. Usually, a certain amount of low mobility charge exist in these materials, at their interface or on their surface. These charges could be process related or can be generated with optical or thermal excitation during the operation of the device. When voltages are applied to the electrodes, charge starts to move and modifies the electric field applied to the optical guides. As a result, modulation characteristics change. This behavior can be modeled using an electrical network approach [65]. Each layer in the device can modeled by an equivalent resistance representing the flow of charge through it, and each interface can modeled by a capacitance representing the potential for charge storage. Such models are able to describe experimental observations successfully [65]. Usual method of preventing such drift involve controlling the resistivity of the buffer and matching it to the resistivity of waveguide layers and modifying the $LiNbO_3$ surface before depositing the buffer layer.

The electrooptic effect in $LiNbO_3$ depends on the polarization of the light, and high-speed modulators are polarization dependent. However, polarization-independent $LiNbO_3$ have been demonstrated. They usually take advantage of the anisotropic electrooptic tensor of $LiNbO_3$. One approach relies on TE/TM mode coupling via off diagonal elements of the electrooptic tensor [66]. In another approach, a $\Delta\beta$ coupler is used [67]. There have been other novel approaches using crossing waveguides and specially designed directional couplers [68], [69]. Digital optical switches can also be used as a polarization-independent modulators [70]. Polarization-independent modulators usually require special crystal cuts and electrode geometries. As a result, the electrooptic coefficient used is not the largest, and the electrode is not suitable for high-speed operation. This makes the efficiency and speed of such devices low.

Linearization of the modulator transfer function has also been studied extensively. Mach–Zehnder modulators have inherently nonlinear characteristic, but this characteristic is very well defined. One can use two modulators and cancel certain harmonics by controlling the optical power, bias, and amplitude and phase of the modulating signal to the modulators. There are several different schemes proposed to achieve that and a comprehensive treatment can be found in [71]. For all linearization schemes, a major concern is the bandwidth of operation. Since in most schemes precise control of applied voltages is needed, it is difficult to get broad-band operation. A recent work discusses this issue and compares the bandwidths of different schemes [72]. At the present time, broad-band linear modulators is an important research area.

2) GaAs/AlGaAs Traveling-Wave Modulators: III–V compound semiconductors such as GaAs, InP, and their alloys have excellent optical properties due to their direct and tunable bandgap and are materials of choice in many optoelectronic components such as lasers and detectors. They also lack inversion symmetry and possess an electrooptic coefficient. As a result, they are also used in modulator applications. The most commonly used optical structure is a Mach–Zehnder interferometer. There are many different ways of making optical waveguides in III–V compound semiconductors. It is possible to adjust the index of refraction of these materials by controlling the composition of their alloys. For example, increasing Al composition x in $Al_xGa_{1-x}As$ compound semiconductor decreases its index of refraction. Furthermore, $Al_xGa_{1-x}As$ is lattice matched to GaAs for all x values. By growing such layers epitaxially using techniques such as molecular beam epitaxy (MBE) or metal organic chemical vapor deposition (MOCVD), it is possible to sandwich a higher index material between two lower index materials. This forms a slab waveguide and provides waveguiding in the vertical direction. The most common approach to provide lateral waveguiding is to etch a rib and form what is known as a rib waveguide. The effective index under the rib is higher than the effective index outside the rib in the etched regions. This provides a lateral index step and a two-dimensional waveguide is formed. There are many other ways to provide waveguiding, which include proton implantation, buried heterostructures, p-n junctions, and disordering. However, rib waveguides are almost the universal choice since vertical and lateral index profiles and dimensions can be independently and precisely controlled. Typical rib widths are in the 2–4-μm range and rib heights are typically less than 1 μm.

The crystal structure of these III–V materials is $\bar{4}3m$ or Zinc Blende [45]. The most commonly used crystal orientation is (001). In (001)-oriented bulk materials, a vertically applied electric field in the (001) direction increases the index of refraction by Δn in (011) direction and decreases in by Δn in $(01\bar{1})$ direction. In other words, index increases along one of the two mutually orthogonal directions parallel to the surface of the crystal. It decreases by the same amount in the other orthogonal direction. Crystals can easily be cleaved along these directions. No index change is observed in (001) direction, which implies that a vertically applied electric field to an (001)-oriented crystal will only modulate the TE mode of the optical waveguide in which the main electric-field component of the optical mode is either in (011) or $(01\bar{1})$ directions; in other words, it is tangential to the surface. No modulation will result for the TM mode that has its main electric-field component in (001) direction, i.e., normal to the surface of

the crystal. The observed index change is

$$\Delta n = \pm \frac{1}{2} n^3 r_{41} F \tag{17}$$

where F is the applied electric field and n is the index of refraction, whose value is about 3.4. r_{41} is the only nonzero bulk electrooptic coefficient and its value is about 1.4 pm/V. This coefficient is about 20 times less than that of $LiNbO_3$, however, net index change for a given electric field is only about five times less due to higher index of refraction of the semiconductor. It is possible to strongly enhance this index modulation using other physical effects. In bulk material operating close to the bandgap of the material and utilizing index changes due to depletion of high levels of doping, much larger index changes approaching 0.001 were observed [73]. Another commonly used approach is to utilize QCSE in a QW structure [14]. Earlier, use of QCSE for EA modulators was described. If the detuning is increased, loss modulation becomes less, but a relatively large index modulation remains. Although modulators using such effects have low drive voltages, they suffer from high optical insertion loss and microwave propagation loss. Therefore, they are not particularly suitable for traveling-wave designs. As a result, for wide-bandwidth traveling-wave modulators, the most commonly utilized physical effect is the bulk electrooptic effect.

The index of the bulk compound semiconductors is isotropic. Furthermore, the refractive index variation between microwave and optical frequencies is rather small. The optical index of refraction is around 3.4 and the relative dielectric constant at microwave frequencies is about 13, which corresponds to an index of 3.6. Since it is a lot easier to form electrodes on the surface of the crystal, the most commonly used electrode is either a CPW or a coplanar strip line (CPS) structure. The optical signal is entirely confined in the semiconductor, which has a refractive index of about 3.4. On the other hand, the microwave and millimeter-wave electric field fringes into the air and experiences an effective index between that of the air and semiconductor. For example, for a coplanar line of zero conductor thickness, the effective dielectric constant is the arithmetic mean of the dielectric constants of the air and the semiconductor, as indicated earlier in (12). Therefore, the effective dielectric constant is around seven, which corresponds to a microwave index of about 2.65. Therefore, there is about 38% of index mismatch between the optical and microwave signals. This requires about 23% velocity reduction. Therefore, in III–V compound semiconductors, velocity matching requires slowing down of the microwave signal. The most commonly used technique to slow the microwave signal is to use a slow-wave transmission line [74]–[77]. Such lines are obtained by periodically loading a uniform transmission line. The loading element is typically a capacitor. This can be achieved using either doped or undoped epitaxial layers. The following two subsections describe these two approaches.

a) GaAs/AlGaAs traveling-wave modulators using doped epitaxial layers: Fig. 15 shows the schematic of such a traveling-wave Mach–Zehnder modulator [74]. The optical structure is a Mach–Zehnder interferometer utilizing multimode interference sections at the input and output for power splitting and combining. GaAs/AlGaAs epitaxial layer is grown on a semiinsulating (SI) GaAs substrate. Underneath the GaAs core, there is a buried n^+ layer, which acts as a ground plane. The main electrode is a CPS. This electrode is periodically loaded by narrow and small capacitive elements. In [74], the capacitive elements used are the reverse-biased capacitance of a Schottky-i-n junction, as shown in Fig. 15. The advantage of this approach is to utilize the large vertical electric field existing in the reverse-biased Schottky-i-n junction. This field overlaps very well with the optical mode enabling low drive voltages. Furthermore, these capacitive elements do not carry any of the axial currents in the transmission line. Therefore, the resistance per unit length and propagation loss of the loaded line is very close to that of the unloaded line. In this design, the required loading capacitance can be expressed as [74]

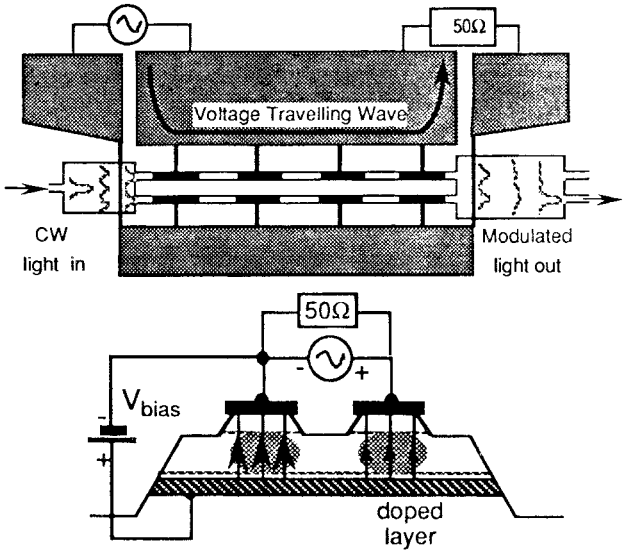

Fig. 15. Schematic of traveling-wave Mach–Zehnder modulator using capacitively loaded CPS [75, Fig. 1]. ©1995 IEEE.

$$C_L = \frac{n_o^2 - n_\mu^2}{cZ_0 n_o} \tag{18}$$

where n_o and n_μ are the optical and microwave indexes, c is the speed of light in vacuum, and Z_0 is the characteristic impedance of the loaded line. In GaAs for a coplanar electrode, a loaded line impedance of 50 Ω, and using the previously quoted values, one obtains $C_L \cong 0.9$ pF/cm. This value is about a factor of 4–5 times smaller than the capacitance of a typical reverse biased Schottky-i-n junction. Therefore, to obtain impedance and velocity matching, the length of the loading elements need to be reduced. This makes only a fraction of the total electrode length electrooptically active, increasing the drive voltage of the modulator. Part of this difficulty can be circumvented using a series push–pull drive, illustrated in Fig. 16. In this case, arms of the Mach–Zehnder interferometer are connected in series. Hence, half the applied voltage drops across each arm, but total loading capacitance is also half of the loading capacitance of each arm. However,

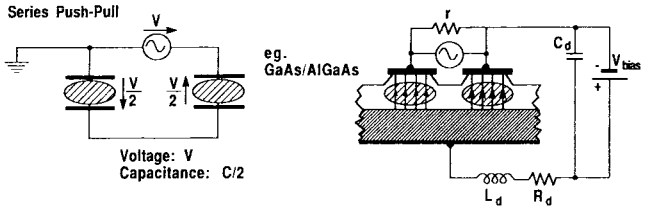

Fig. 16. Series push–pull drive for the modulator shown in Fig. 15. Phase modulator arms are modeled as capacitors [74, Fig. 3(b)]. ©1991 IEEE.

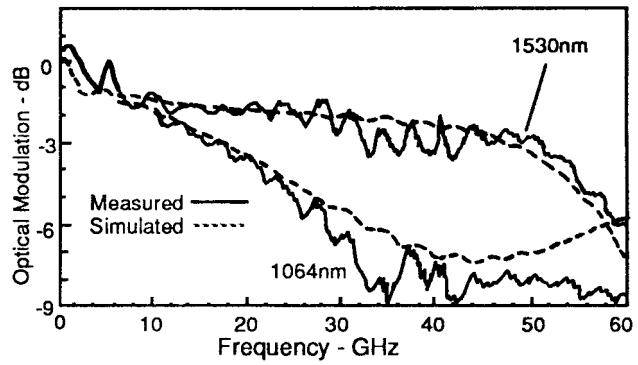

Fig. 17. Measured frequency response of a traveling-wave modulator using loaded line design in which loading elements are reverse-biased Schottky-i-n junctions [75, Fig. 2]. ©1995 IEEE.

this bias scheme also requires bias and decoupling circuitry, as illustrated in Fig. 16. It is not possible to use a full or parallel push–pull bias in this scheme because of the continuous n^+ layer underneath the arms of the interferometer. Such devices with a total of 1-cm electrode length and loading segment lengths of 0.5, 0.6, and 0.7 mm were fabricated and characterized [74]. dc V_π values at 1.15 μm for 0.5-, 0.6-, and 0.7-mm segment-length electrodes were 5.7, 4.25, and 4.24 V, respectively. Corresponding bandwidths were $>$26.5, 25.0 and 22.5 GHz, respectively. As the segment length gets longer, more of the electrode becomes electooptically active and drive voltage reduces. On the other hand, capacitive loading becomes excessive and it becomes difficult to obtain impedance and velocity matching. As a result, the device bandwidth decreases. Such slow-wave electrodes are inherently low-pass filters. The upper end of the passband is determined by the Bragg frequency of the slow-wave geometry and depends on the periodicity of loading elements. It is possible to push this frequency to very high values by making the period of loading elements very short. It is observed that for long-period devices, the upper frequency cutoff becomes very sharp and abrupt. On the other hand, short-period devices have a much more gradual frequency rolloff [74]. Recently, such a device demonstrated an electrical 3-dB bandwidth of 50 GHz and V_π of 13 V at 1530 nm [75]. Modulation response of such a device is shown in Fig. 17.

b) GaAs/AlGaAs traveling-wave modulators using undoped epitaxial layers: Another approach for GaAs traveling-wave modulator design is to use unintentionally doped epitaxial layers [76], [77]. Such GaAs/AlGaAs layers self deplete due to Fermi level pinning at the surface and the depletion originating at the SI substrate interface and behave very

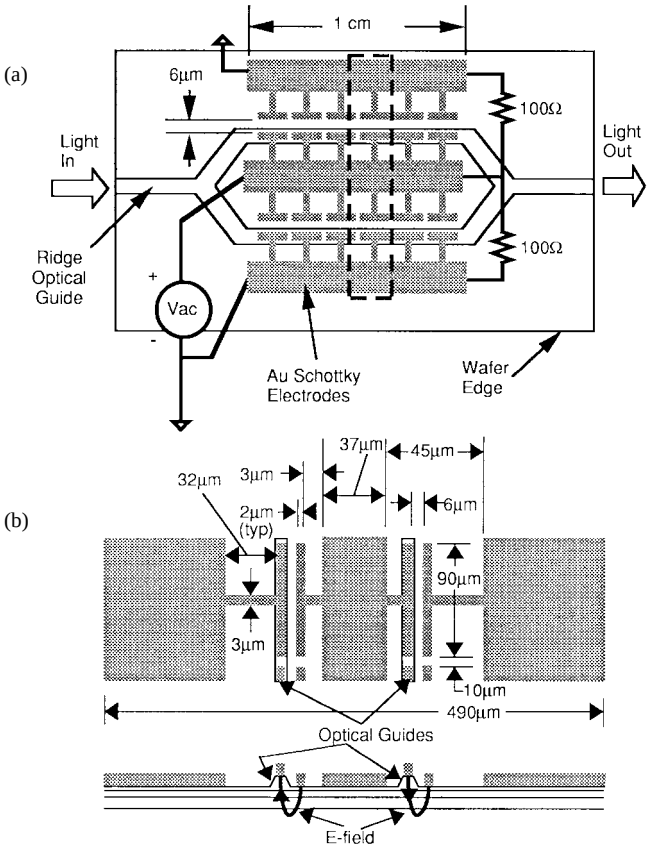

Fig. 18. (a) Top-view schematic of a GaAs/AlGaAs modulator using unintentionally doped layers. (b) Top-view schematic of the modulator section delineated by the dashed line in (a) together with a cross-sectional schematic [76, Figs. 1 and 2]. Reproduced by permission of the Institution of Electrical Engineers.

similar to low-loss dielectric materials. As a result, optical and microwave losses become very low. The required velocity slowing can be achieved using a properly designed electrode. A schematic of such a device is shown in Fig. 18. The optical structure is a Mach–Zehnder interferometer. A (001)-oriented GaAs/AlGaAs heterostructure grown by MBE on SI GaAs provides vertical optical waveguiding. The lateral waveguiding is obtained by etching ridges down into the top AlGaAs layer. The microwave electrodes are fabricated by evaporating 200 Å/200 Å/1 μm of Ti/Pt/Au. This forms a Schottky contact with the epitaxial layers. A voltage applied between the electrodes biases two back-to-back Schottky diodes. The conductivity of self-depleted epilayers is so low that, for frequencies larger than 1 MHz or even lower, the epilayers start to behave like slightly lossy dielectrics. Hence, the situation becomes identical to electrodes on an insulating dielectric. This makes it possible to apply mainly (001)-directed electric fields of opposite polarity on the optical guides, as shown in Fig. 18. This generates phase shifts of opposite sign on both arms through the linear electrooptic effect, creating a net differential phase shift between the arms of the interferometer. Hence, push–pull modulation results. The device electrode is a modified coplanar line, in which T-rails stem from either side of the center conductor and from the inner side of the both ground planes [78]. These T-rails

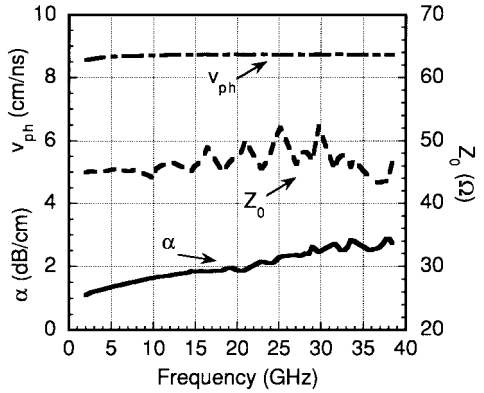

Fig. 19. Measured microwave characteristics of the modulator electrode of the device shown in Fig. 18 [78, Fig. 2]. Reproduced by permission of the Institution of Electrical Engineers.

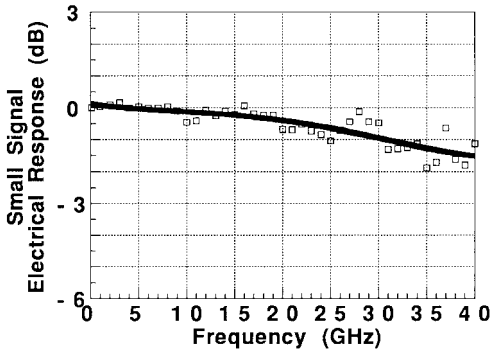

Fig. 20. Measured small-signal response of the modulator shown in Fig. 18 at 1.55 μm [76, Fig. 4]. Reproduced by permission of the Institute of Electrical Engineers.

form tiny capacitors, which periodically load the line, increase its capacitance per unit length, and, thus, slow the microwave signal propagating on the electrode. For this structure, axial transmission-line currents cannot flow along these T-rails. Only displacement current flows in these tiny capacitors. Therefore, current crowding and the microwave loss is determined by the distance between the center conductor and ground plane of the unloaded line. One can make that gap large to keep microwave loss low [78]. On the other hand, the gap between the T-rails determine the field applied to the optical guides for a given voltage. In this design, this gap can be reduced significantly with a very small increase in the microwave loss [78]. As a result, the electrode gap has been decoupled from the electrode loss.

Fig. 19 shows the measured characteristics of the modulator electrode used in the experiments described later [78]. In this case, the small gap between the T-rails is 6 μm. The measured phase velocity shows virtually no dispersion and is within 1% of the target value. The characteristic impedance is 46 Ω, which is very close to the target value of 50 Ω. The microwave loss is also very low. It increases with frequency and approaches a value of 3 dB/cm at 40 GHz. This value is considerably less than the 6.34-dB loss limit that determines the 3-dB electrical bandwidth when velocity and impedance matching is obtained. Therefore, a very high electrical bandwidth is expected from this device. Another advantage of this design is the symmetry of the high field region and the large segmentation factor. The 6-μm gap extends over 90% of the electrode length. The increase in the microwave loss of the unperturbed coplanar line due to the presence of the T-rails is measured to be less than 1 dB over the entire frequency range. It is possible to reduce the gap further. A T-rail gap of 3 μm results in a microwave loss of 4.3 dB/cm at 35 GHz [78]. Although loss increases, its absolute value is still very low. Such small gap values make this geometry suitable for both directional-coupler- and Mach–Zehnder-type electrooptic modulators.

The small-signal electrical bandwidth of this device at 1.55 μm is shown in Fig. 20. The bandwidth at 1.55 μm is in excess of 40 GHz. It is basically flat up to 20 GHz and starts to roll off gradually and becomes about 1.5–2 dB down at 40 GHz. Extrapolating the curve fit the bandwidth was estimated to be between 50 to 60 GHz. Although this is a rather high bandwidth, it is still less than the bandwidth expected based on the electrode data. At 1.3 μm, the 3-dB bandwidth was measured to be about 37 GHz [77], [79]. This is considerably less than what is expected. The reason for this discrepancy was shown to be the matching of wrong velocities; namely, matching of phase velocity rather than group velocity. This makes a lot of physical sense because once the optical signal starts to interact with the electrical signal, it is no longer a single-frequency waveform. It is clearly phase modulated and this phase-modulated waveform travels with the group velocity. This velocity should be the same as the group velocity of the electrical waveform so that they keep interacting and the phase modulation accumulates. Therefore, group velocities should be matched. Since the electrode is a quasi-TEM transmission line, it has no dispersion and phase and group velocities are the same. This is also obvious from the measured data. However, for the optical guide, phase and group velocities are different. The actual group-velocity mismatch turns out to be 10% at 1.3 μm and 5% at 1.55 μm, which explains the measured bandwidths. Actually, this experimental observation is consistent with the claims made on one of the early publications on this topic [80]. This is a very important point, especially for semiconductor modulators where material index dispersion is much more significant, especially close to the band edge. Therefore, providing the right kind of velocity match is very important to get the widest possible bandwidth in traveling-wave modulators.

V_π of this modulator was 14 V at 1.3 μm and 16.8 V at 1.55 μm. These values are high for a high-speed modulator. The source of this difficulty is the poor overlap of the vertical component of the applied electric field with the optical mode. As the electrode gap gets smaller, applied field intensity increases. However, field lines start to become more tangential to the surface and the increase in its vertical component is not as much. One way to improve the overlap is to use a doped layer, as in [74]. However, this results in excessive capacitance, which reduces fill factor and true push–pull operation becomes impossible. A promising approach is to use substrate removed waveguides and process both sides of the

epilayer [81]. This should yield very high-speed devices with low drive voltages when combined with the undoped epilayer approach.

GaAs modulators can handle very large amounts of optical powers since they are very similar to semiconductor lasers that generate very high optical powers [82]. Practical limit to the power-handling capability is the catastrophic facet damage. Bias stability is also not a major issue for good quality material. The issues related to the linearity of III–V electrooptic modulators is the same as $LiNbO_3$ modulators.

Polarization-independent operation of III–V electrooptic modulators can be achieved either designing the material using appropriate amount of strain or using novel device ideas. Strain may provide equal electrooptic coefficient for TE and TM modes, making the operation the same for two orthogonal polarizations. In bulk material, it is possible to get TE/TM coupling for certain applied field orientations. In one approach, polarization dependence was obtained using near degenerate TE and TM modes and controlling the coupling between them [83]. In this case, electrodes were suitable for traveling-wave operation [84] and such a device has potential for broad-band polarization-independent operation.

3) Polymer Traveling-Wave Modulators: Organic polymers have many attractive features for integrated optical applications [85]. It is possible to form multilayer polymer stacks by spin deposition and curing on a large variety of substrates or even on fabricated circuits [86]. They can be patterned using several different techniques such as photo bleaching and reactive ion etching. They present good optical properties, such as low propagation loss and low index of refraction very close to that of the single-mode fiber. They also have low dielectric constant, which is important for high-speed devices. These properties resulted in passive low-loss polymer optical waveguides that can couple to single-mode optical fibers very efficiently [87], [88].

Polymers can also be made electrooptic and used in active devices. Certain molecules known as chromophores possess large ground-state electric dipole moments and exhibit large optical nonlinearities. This microscopic nonlinearity can be converted to a macroscopic nonlinearity by mixing them with polymers and aligning their dipole moments. The most common method is to take a chromophoric polymer film and apply a strong electric field across it while keeping the film heated at a high temperature near its glass transition temperature. At such high temperatures, randomly aligned individual chromophores are able to move in the polymer and align themselves with the externally applied electric field due to their dipole moments. After this alignment, if the film is cooled to room temperature while applied electric field is present, ordering of chromophores is achieved. This creates a macroscopic nonlinearity that can be used for electrooptic modulation. This process is known as high-temperature poling. Poling temperatures and fields depend on the particular film, but are typically about 100 °C–200 °C and 100–200 V/μm.

Most common techniques of poling a polymer film is either corona or electrode poling. In corona poling, corona discharge is used to create large poling fields over large areas. In electrode poling, one approach is to spin coat the lower cladding and core on a ground electrode. Then poling electrodes are formed on top of the cladding. After poling, these electrodes are removed and the upper cladding is spin coated. Alternatively, whole stack can be spin coated, followed by poling electrode formation, poling, and removal of poling electrodes. The conductivity of upper and lower cladding regions of the polymer waveguide should be larger than the core of the waveguide for most of the poling voltage to drop across the electrooptic core and result in effective poling. Usually, the electrooptic coefficient increases linearly with poling field, but so does the optical loss and birefringence.

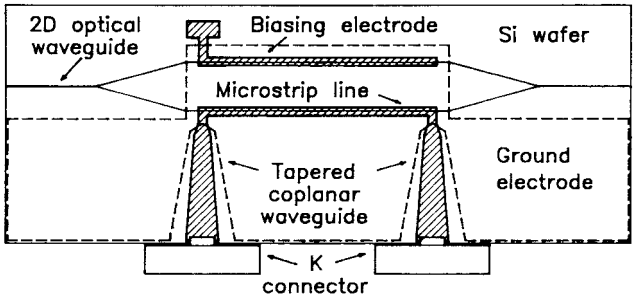

Fig. 21. Schematic view of a polymeric traveling-wave modulator [92, Fig. 1]. Reproduced by permission of the American Institute of Physics.

After poling, electrooptic activity is observed. For modulating fields applied in the poling-field direction, two different electrooptic coefficients are observed, depending on the polarization of the optical mode. The coefficient for TM polarization, i.e., when the optical field is polarized in the modulating field direction, is r_{33}. The coefficient for TE polarization, i.e., when the optical field is polarized perpendicular to the modulating field direction, is r_{13}. Typically for polymers, r_{33} is about three times larger than r_{13}. At the current time, for most of the reported modulators, r_{33} values range between 1–20 pm/V, although values as high as 67 pm/V have been reported [89]. The index change for an applied electric field is given by (10). Polymer indexes of refraction are around 1.6, which makes a polymer with $r_{33} \cong 12$ pm/V equivalent to bulk GaAs as far as index change is concerned. To take advantage of high r_{33}, the modulating field should be applied in the poling-field direction and the optical mode should be polarized in the same direction. For these considerations, the most commonly used electrode is microstrip and the optical polarization is TM.

Fig. 21 shows a traveling-wave polymer modulator [92]. The optical structure is the Mach–Zehnder interferometer. The optical waveguides were fabricated by spin coating three layers of polymers that act as claddings and the core of the optical waveguide onto a high-resistivity Si wafer, which was coated with a patterned gold-plated film. Exposing the polymer film to a high-intensity light at the appropriate wavelength reduces the refractive index in the exposed areas, which is known as photobleaching. After poling, photobleaching was used to form channel optical waveguides. The thickness of the polymer stack was 6.5 μm. Tapered coplanar lines were used to couple in and out of the 12-mm-long microstrip electrode. V_π of this modulator was 10 V. Low dielectric constant and low dielectric-constant dispersion of polymers from microwave

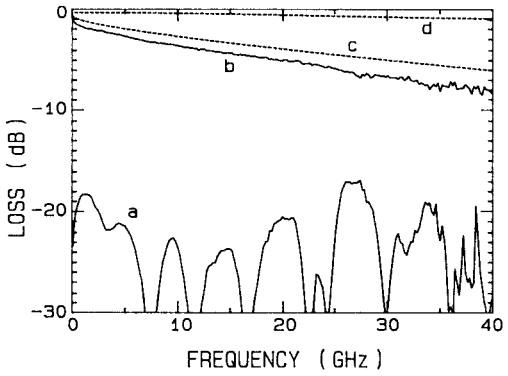

Fig. 22. Microwave power loss as a function of frequency of the modulator electrode shown in Fig. 21. a is the return loss, b is the transmission loss, c is the loss of the 12-mm-long electrode, and d is the coupling loss [92, Fig. 2]. Reproduced by permission of the American Institute of Physics.

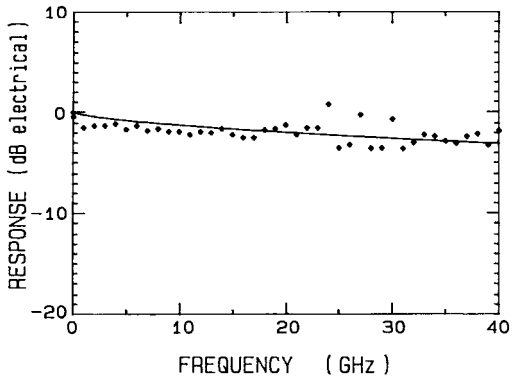

Fig. 23. Frequency response of the small-signal optical modulation of the device shown in Fig. 21 [92, Fig. 3]. Reproduced by permission of the American Institute of Physics.

to optical frequencies offer an advantage in the design of traveling-wave modulators. It is possible to get very good velocity matching using a microstrip electrode. For example, using a commonly quoted value of 1.6 for the optical index and 2.9 for the microwave relative dielectric constant and a 10-μm-thick polymer stack, a 50-Ω microstrip line would have about 25-μm strip width and less than 5% velocity mismatch. In the case of the modulator shown in Fig. 21, index mismatch was estimated to be 0.03. Electrode loss and modulation response as a function of frequency are shown in Figs. 22 and 23. The bandwidth is wider than 40 GHz. Other polymer modulators with bandwidths wider than 40 GHz have been reported [90], [91]. Furthermore, polymer modulators operating at W-band (75–110 GHz) have been reported, demonstrating intrinsic high-frequency response of electrooptic polymers [90], [91].

If corona poling or a single-poling electrode is used, chromophores in both arms of the Mach–Zehnder are aligned in the same direction. This makes it difficult to make a push–pull modulator using a single microstrip electrode and usually only one arm of the interferometer is phase modulated [92], [93]. It is possible to use two electrodes driven 180° out-of-phase on both arms of the interferometer to get push–pull operation and halve the drive voltage. This requires a broadband 3-dB microwave hybrid and makes only half the power available to each arm without considering the loss of the

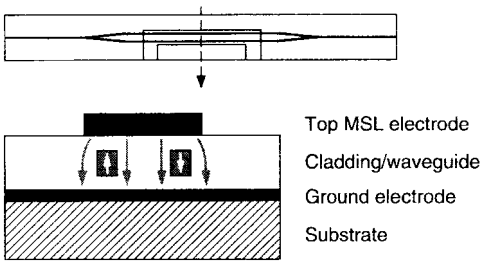

Fig. 24. Top and cross-sectional views of the device showing the optical push–pull operation in a polymer electrooptic Mach–Zehnder modulator and a single microstrip-line driving circuit. The white and gray arrows represent poling and modulation field directions, respectively [94, Fig. 1]. ©1999 IEEE.

hybrid. Another way of obtaining push–pull operation is to pole the arms of the Mach–Zehnder in opposite directions, as shown in Fig. 24 [94]. In this case, poling electrodes had to be closely spaced in order to form a 50-Ω microstrip line. The polymer stack is about 10-μm thick, which makes the required microstrip width about 30 μm, and implies that the separation between the arms of the interferometer should be less than that. Therefore, the poling electrodes should be less than 30 μm apart. Since voltages approaching 1000 V must be applied to create poling fields in the range 100 V/μm across the 10-μm film, the air breakdown between closely spaced poling electrodes becomes an issue. In this case, this difficulty was addressed by using a fused silica piece on top of the poling electrodes to modify the field distribution in the gap, and the sample was placed in an inert gas (SF_6) ambient to increase the breakdown field. Modulators with 2-cm-long microstrip electrodes had V_π values of 40 and 20 V for one arm and push–pull operation, respectively, at 1.3 μm [94]. This corresponds to an r_{33} value of about 7 pm/V. The typical loss of a pigtailed modulator was about 12 dB. 6 dB of the loss was attributed to the on-chip optical loss of the 3-cm-long interferometer and the rest was due to mode mismatch between the fiber and optical waveguide. The additional processing associated with poling electrode formation can be eliminated if device electrodes can be used as poling electrodes. By applying 180° out-of-phase pulsed voltages to the electrodes, it is possible to pole both arms of the interferometer sequentially [95]. In this way, the maximum voltage between the electrodes is reduced from $2V_p$ in the case of dc poling to V_p in the case of pulse poling, where V_p is the poling voltage applied across one arm of the interferometer. The field strength between the device electrodes during poling can be further reduced by increasing the separation between electrodes. One approach uses to parallel microstrip lines of 100-Ω characteristic impedance each [96]. This way, it was possible to get a separation of 200 μm between the arms of the interferometer.

Chromophores used in electrooptic polymers have certain optical transitions in the wavelength range used in optical applications. For example, it is reported that Disperse Red 19 (DR19) chromophores have a peak absorption wavelength around 470 nm corresponding to $\pi - \pi^*$ transition [97]. Therefore, any optical energy present around this wavelength excites the chromophore, which looses its orientation when it relaxes. This results in photoinduced relaxation, which

reduces the electrooptic coefficient, absorption, and optical index. This effect is shown to be polarization dependent due to large optical dipole moment associated with the chromophore. At wavelengths away from the absorption peak, this effect decreases significantly. However, optical nonlinearity of the material results in second harmonic generation, which, in turn, generates optical power within the absorption band even for near infrared excitations [98]. Typically, second harmonic generation efficiency in commonly used optical waveguides is very low due to poor phase matching. Nevertheless, this places an upper limit on the maximum power-handling capacity of the optical waveguide. For example, at 1320 nm for 10 mW in a 10-μm^2 cross-section waveguide, device lifetime is estimated to be larger than 10^4 h for a 30% decay in the electrooptic efficiency [97]. On the other hand, lifetime at 1064 nm was estimated to be $\sim$1 h due to 532-nm second harmonic [97]. Recently, double-end cross-linked polymers were found to stable when exposed to 250 mW at 1.32 μm for one week [99]. They were also found thermally stable when baked at 100 °C in air for more than 2000 h. r_{33} of these materials are quoted to be 6 pm/V.

Long-term bias stability is another very important concern. Polymer layers have finite conductivity, which effect electrical response under dc and ac applied biases. This effect was studied using an equivalent-network approach [65], [100], [101]. Every layer of the optical waveguide can be modeled as a parallel *RC* circuit. Resistance and capacitance of each layer depend on its conductivity σ and dielectric constant ε, respectively. At low frequencies and low dc biases, the fraction of the applied voltage across the electrooptically active core layer depend on the relative conductivity of the layers. For low-bias operation, conductivity of the electrooptic layer is desired to be much smaller than the other layers. This condition is also required for effective poling. However, it is shown that this would generate a bias drift that depends on the amplitude of the ac voltage swing. This could be a problem in practical operation, requiring continuous bias-point monitoring and adjustment. This effect has a ω^{-1} dependence and can be made zero by matching the relaxation constants (σ/ε) for all layers [100].

At the current time, the electrooptic polymer topic is a very intense research area. One direction is to improve material-stability and electrooptic properties of polymers. Another direction seems to be the elimination of high-temperature electric-field poling. This would enable room-temperature processing, but requires electrooptically active or ordered material to start with. This can be achieved by depositing the polymer film monolayer by monolayer using Langmuir–Blodgett films and relying on self-ordering of the chromophores in each monolayer.

D. Traveling-Wave EA Modulators

As described at the conclusion of Section III-A, one of the emerging research directions in EA device research is to reduce the drive voltage and increase the bandwidth. Lumped device performance seems to be saturated around 2-V drive voltage and 50-GHz bandwidth. The main reason for that is the conflicting requirements on the length of the device. Low drive voltages require longer devices, yet wide bandwidths require shorter devices. One way to address this problem is to design the device as a traveling-wave modulator. For a traveling-wave device, the *RC* time constant is not the bandwidth limit, and the device can be made longer without sacrificing bandwidth. However, the special structure of an EA modulator presents interesting issues. First of all, the optical propagation loss of the EA device is rather high. Therefore, increasing the length over a few hundred micrometers introduces excessive loss, which may negate the effect of improved slope efficiency in the link design. It is argued that optimum device length for maximum link efficiency is around 200 μm [102]. Large device capacitance per unit length also makes it difficult to make a 50-Ω transmission line with matched velocity. Since the device is rather short, velocity matching is not an issue up to frequencies well into the submillimeter-wave range. The bandwidth is typically limited by the microwave loss [103]. For TW-EA modulator electrodes, measured microwave loss coefficients of about 60–80 dB/cm at 40 GHz were reported [103]. This excessive loss is due to heavily doped layers inside the device and is another factor limiting the length of the device. Characteristic impedance values are approximately 25 Ω [103], [104]. However, designing the device as part of a 25-Ω transmission line makes longer devices possible and packaging easier. Recently, a 200-μm-long TW-EA device with a bandwidth over 54 GHz [105] and a 300-μm-long device with a bandwidth of 25 GHz [104] were reported. Both devices were polarization insensitive and operated at 1.55 μm. For 20-dB on/off ratio, drive voltage of the 200 and 300 μm devices were 3 and 1.9 V, respectively.

IV. SUMMARY

Recent developments in high-speed lasers resulted in small-signal bandwidths exceeding 40 and 25 GHz at 1.1- and 1.55-μm wavelengths, respectively. Further improvements in the slope efficiency and RIN of these lasers may make them attractive candidates for directly modulated links. Lumped EA modulator modules with electrical bandwidths approaching 60 GHz and drive voltages around 2 V for 20-dB extinction have also been demonstrated at 1.55 μm. Similar devices with bandwidths approaching 40 GHz have also been fabricated at 1.3 μm. Their fiber-to-fiber insertion loss is around 10 dB and polarization-independent operation has been achieved. Improved material design is expected to improve power-handling capability. Wavelength and temperature dependence of the transmission characteristics can be stabilized using novel schemes taking advantage of device characteristics. Suppression of certain intermodulation products also seems to be possible using wavelength dependence of the optical transmission. Drive voltage and bandwidth can be improved further using TW-EA modulator approach. Traveling-wave $LiNbO_3$ modulators offer stable devices that can handle large optical powers. Such modulators with electrical bandwidths as high as 75 GHz and V_π around 5 V have been demonstrated. Their fiber-to-fiber insertion loss is around 5 dB. Further V_π reduction is being pursued. GaAs modulators also offer

stable operation and the ability to handle large optical powers. Electrical bandwidths up to 50 GHz have been realized. V_π values are around 15 V and fiber-to-fiber insertion loss is in the 10–15-dB range. Efforts to reduce the drive voltage and fiber-to-fiber insertion using novel processing techniques are under way. Polymer modulators offer flexible and low-cost technology. High-speed capability of electrooptic polymers have been demonstrated. Polymer modulators with electrical bandwidths exceeding 40 GHz have been reported. V_π values are around 10 V and fiber-to-fiber insertion loss is about 10 dB. Bias stability, power-handling capability, and material-stability issues are still under examination. In all traveling-wave designs, broad-band linearization of the transfer characteristics and polarization-independent operation remain as challenges for device researchers.

ACKNOWLEDGMENT

The author thanks C. Ozturk and S. Sakamoto for their help with the figures.

REFERENCES

[1] C. Cox III, E. Ackerman, R. Helkey, and G. Betts, "Techniques and performance of intensity modulation direct detection analog optical links," *IEEE Trans. Microwave Theory Tech.*, vol. 45, pp. 1375–1383, Aug. 1997.

[2] D. Tauber and J. E. Bowers, "Dynamics of wide bandwidth semiconductor lasers," *Int. J. High Speed Electron. Syst.*, vol. 8, no. 3, pp. 377–416, 1997.

[3] L. A. Coldren and S. W. Corzine, *Diode Lasers and Photonic Integrated Circuits*. New York: Wiley, 1995.

[4] S. Weissner, E. C. Larkins, K. Czotscher, W. Benz, J. Daleiden, I. Esquivias, J. Fleissner, J. D. Ralston, B. Romero, R. E. Sah, A. Schonfelder, and J. Rosenweig, "Damping limited modulation bandwidths up to 40 GHz in undoped short cavity $In_{0.35}Ga_{0.65}As$-GaAs multiple quantum well laser," *IEEE Photon. Technol. Lett.*, vol. 8, pp. 608–610, May 1996.

[5] R. Olshansky, P. Hill, V. Lanzisera, and W. Powazinik, "Universal relationship between resonant frequency and damping rate of 1.3 μm InGaAsP semiconductor lasers," *Appl. Phys. Lett.*, vol. 50, pp. 653–655, 1987.

[6] M. Willatzen, A. Uskov, J. Mork, H. Olesen, B. Tromborg, and A. P. Jauho, "Nonlinear gain suppression in semiconductor lasers due to carrier heating," *IEEE Photon. Technol. Lett.*, vol. 3, pp. 606–609, July 1991.

[7] W. Rideout, W. F. Sharfin, E. S. Koteles, M. O. Vassell, and B. Elman, "Well-barrier hole burning in quantum well lasers," *IEEE Photon. Technol. Lett.*, vol. 3, pp. 784–786, Sept. 1991.

[8] R. Nagarajan, T. Fukushima, S. W. Corzine, and J. E. Bowers, "Effects of carrier transport on high speed quantum well lasers," *Appl. Phys. Lett.*, vol. 59, pp. 1835–1837, 1991.

[9] R. Nagarajan, M. Ishikawa, T. Fukushima, R. S. Geels, and J. E. Bowers, "High-speed quantum well lasers and carrier transport effects," *IEEE J. Quantum Electron.*, vol. 28, pp. 1990–2008, Oct. 1992.

[10] P. A. Morton, T. Tanbun-Ek, R. A. Logan, N. Chand, K. Wecht, A. M. Sergent, and P. F. Sciortino Jr., "Packaged 1.55 μm DFB laser with 25 GHz modulation bandwidth," *Electron. Lett.*, vol. 30, pp. 2044–2046, 1994.

[11] P. A. Morton, R. A. Logan, T. Tanbun-Ek, P. F. Sciortino Jr., A. M. Sergent, R. K. Montgomery, and B. T. Lee, "25 GHz bandwidth 1.55 μm GaInAsP p-doped strained multiquantum well lasers," *Electron. Lett.*, vol. 28, pp. 2156–2157, 1992.

[12] C. H. Cox III, H. V. Roussell, R. J. Ram, and R. J. Helkey, "Broadband, directly modulated analog fiber link with positive intrinsic gain and reduced noise figure," in *Proc. IEEE Int. Topical Meeting Microwave Photon.*, Princeton, NJ, Oct. 12–14, 1998, pp. 157–160.

[13] S. G. Ayling, D. R. Wright, M. B. Allenson, K. P. Hilton, and G. W. Smith, "Novel integrated laser devices with greatly enhanced quantum efficiency and intrinsic RF matching for low loss broad-band optomicrowave applications," in *Proc. IEEE Int. Topical Meeting Microwave Photon.*, Princeton, NJ, Oct. 12–14, 1998, pp. 161–164.

[14] D. A. B. Miller, D. S. Chemla, T. C. Damen, A. C. Gossard, W. Wiegmann, T. H. Wood, and C. A. Burrus, "Electric field dependence of optical absorption near the bandgap of quantum well structures," *Phys. Rev. B, Condens. Matter*, vol. 32, no. 2, pp. 1043–1060, 1985.

[15] K. Wakita, I. Kotaka, H. Asai, S. Nojima, and O. Mikami, "High efficiency electroabsorption in quaternary AlGaInAs quantum well optical modulators," *Electron. Lett.*, vol. 24, pp. 1324–1326, 1988.

[16] T. Ido, H. Sano, D. J. Moss, S. Tanaka, and A. Takai, "Strained InGaAs/InAlAs MQW electroabsorption modulators with large bandwidth and low driving voltage," *IEEE Photon. Technol. Lett.*, vol. 6, pp. 1207–1209, Oct. 1994.

[17] T. Ido, H. Sano, S. Tanaka, D. J. Moss, and H. Inoue, "Performance of strained InGaAs/InAlAs multiple quantum well electroabsorption modulators," *J. Lightwave Technol.*, vol. 14, pp. 2324–2331, Oct. 1996.

[18] G. Bastard, E. E. Mendez, L. L. Chang, and L. Esaki, "Variational calculations on a quantum well in an electric field," *Phys. Rev. B, Condens. Matter*, vol. 28, pp. 3241–3245, 1983.

[19] F. Devaux, F. Dorgeuille, A. Ougazzaden, F. Huet, M. Carenco, M. Henry, Y. Sorel, J. F. Kerdiles, and E. Jeanney, "20-GBit/s operation of a high efficiency InGaAsP/InGaAsP MQW electroabsorption modulator with 1.2-V drive voltage," *IEEE Photon. Technol. Lett.*, vol. 5, pp. 1288–1290, Nov. 1993.

[20] K. Wakita, I. Kotaka, O. Motomi, H. Asai, Y. Kawamura, and M. Naganuma, "High-speed InGaAlAs/InAlAs multiple quantum well optical modulators," *J. Lightwave Technol.*, vol. 8, pp. 1027–1032, July 1990.

[21] K. Wakita, K. Yoshino, I. Kotaka, S. Kondo, and Y. Noguchi, "Blue chirp electroabsorption modulators with very thick quantum wells," *IEEE Photon. Technol. Lett.*, vol. 8, pp. 1169–1171, Sept. 1996.

[22] T. Ido, S. Tanaka, M. Suzuki, M. Koizumi, H. Sano, and H. Inoue, "Ultra high-speed multiple quantum well electroabsorption optical modulators with integrated waveguides," *J. Lightwave Technol.*, vol. 14, pp. 2026–2034, Sept. 1996.

[23] K. K. Loi, I. Sakamoto, X. B. Mei, C. W. Tu, and W. S. C. Chang, "High efficiency 1.3-μm InAsP-GaInP MQW electroabsoprtion waveguide modulators for microwave fiber optic links," *IEEE Photon. Technol. Lett.*, vol. 8, pp. 626–628, May 1996.

[24] S. M. Lord, B. Pezeshki, and J. S. Harris, "Electroabsorption modulators operating at 1.3 μm on GaAs substrates," *Opt. Quantum Electron.*, vol. 25, pp. S953–S964, 1993.

[25] A. Ougazzaden, F. Devaux, E. V. K. Rao, L. Silvestre, and G. Patriarche, "1.3 μm strain compensated InAsP/InGaP electroabsorption modulator structure grown by atmospheric pressure metal organic vapor epitaxy," *Appl. Phys. Lett.*, vol. 70, no. 1, pp. 96–98, 1997.

[26] K. Wakita, I. Kotaka, T. Amano, and H. Sugiura, "1.3 μm waveguided electroabsorption modulators with strain compensated InAsP/InGaP MQW structures," *Electron. Lett.*, vol. 31, no. 16, pp. 1339–1341, 1995.

[27] K. K. Loi, L. Shen, H. H. Wieder, and W. S. C. Chang, "Electroabsorption waveguide modulators at 1.3-μm fabricated on GaAs substrates," *IEEE Photon. Technol. Lett.*, vol. 9, pp. 1229–1231, Sept. 1997.

[28] N. Mineo, K. Yamada, K. Nakamura, S. Sakai, and T. Ushikobo, "60 GHz band electroabsorption modulator module," in *Opt. Fiber Conf.*, San Jose, CA, 1998.

[29] O. Motomi, I. Kotaka, K. Wakita, S. Nojima, K. Kawano, Y. Kawamura, and H. Asai, "40 GHz bandwidth InGaAs/InAlAs multiple quantum well optical intensity modulator," *Appl. Opt.*, vol. 31, pp. 2030–2035, 1992.

[30] K. Satzke, D. Baums, U. Cebulla, H. Haisch, D. Kaiser, E. Lach, E. Kuhn, J. Weber, R. Weinmann, P. Widemann, and E. Zielinski, "Ultrahigh bandwidth (42 GHz) polarization independent ridge waveguide electroabsorption modulator based on tensile strained InGaAsP MQW," *Electron. Lett.*, vol. 31, pp. 2030–2032, 1995.

[31] K. K. Loi, X. B. Mei, J. H. Hodiak, C. W. Tu, and W. S. C. Chang, "38 GHz bandwidth 1.3 μm MQW electroabsorption modulators for RF photonic links," *Electron. Lett.*, vol. 34, pp. 1018–1019, May 1998.

[32] T. H. Wood, J. Z. Pastalan, C. A. Burrus, B. C. Johnson, B. I. Miller, J. L. de Miguel, U. Koren, and M. G. Young, "Electric field screening by photogenerated holes in multiple quantum wells: A new mechanism for absorption saturation," *Appl. Phys. Lett.*, vol. 57, no. 11, pp. 1081–1083, 1990.

[33] D. J. Moss, T. Ido, and H. Sano, "Photogenerated carrier sweep out times in strained $In_xGa_{1-x}As/In_yAl_{1-y}As$ quantum well modulators," *Electron. Lett.*, vol. 30, no. 5, pp. 405–406, 1994.

[34] R. Sahara, K. Morito, and H. Sosa, "Engineering of barrier band structure for electroabsorption MQW modulators," *Electron. Lett.*, vol. 30, no. 9, pp. 698–699, 1994.

[35] R. Sahara, K. Morito, K. Sato, Y. Kotaki, H. Soda, and N. Okazaki, "Strongly improved frequency response at high optical powers from In-

GaAsP compensated strain MQW electroabsorption modulators," *IEEE Photon. Technol. Lett.*, vol. 7, pp. 1004–1006, Sept. 1995.
[36] C. Sun, S. Pappert, R. Welstand, T. Zhu, P. Yu, Y. Liu, and J. Chen, "High supurious-free dynamic range fiber link using a semiconductor electroabsorption modulator," *Electron. Lett.*, vol. 31, pp. 902–903, May 1995.
[37] R. B. Welstand, S. A. Pappert, D. T. Nichols, L. J. Lembo, Y. Z. Liu, and P. K. L. Yu, "Enhancement in electroabsorption waveguide modulator slope efficiency at high optical power," *IEEE Photon. Technol. Lett.*, vol. 10, pp. 961–963, July 1998.
[38] K. Wakita, I. Kotaka, K. Yoshino, S. Kondo and Y. Noguchi, "Polarization independent electroabsorption modulators using strain compensated InGaAs/InAlAs MQW structures," *IEEE Photon. Technol. Lett.*, vol. 7, pp. 1418–1420, Dec. 1995.
[39] F. Devaux, S. Chelles, A. Ougazzaden, A. Mircea, M. Carre, F. Huet, A. Carenco, Y. Sorel, J. F. Kerdiles, and M. Henry, "Full polarization insensitivity of a 20-Gb/s strained MQW electroabsorption modulator," *IEEE Photon. Technol. Lett.*, vol. 6, pp. 1203–1205, Oct. 1994.
[40] T. Yamaguchi, T. Morimoto, K. Akeura, K. Tada, and Y. Nakano, "Polarization independent waveguide modulator using a novel quantum well with mass dependent width," *IEEE Photon. Technol. Lett.*, vol. 6, pp. 1442–1444, Dec. 1994.
[41] M. Kato, K. Tada, and Y. Nakano, "Wide wavelength polarization independent optical modulator based on tensile strained quantum well with mass dependent width," *IEEE Photon. Technol. Lett.*, vol. 8, pp. 785–787, June 1996.
[42] G. L. Li, R. B. Welstand, W. X. Chen, J. T. Zhu, S. A. Pappert, C. K. Sun, Y. Z. Liu, and P. K. L. Yu, "Novel bias control of electroabsorption waveguide modulator," *IEEE Photon. Technol. Lett.*, vol. 10, pp. 672–674, May 1998.
[43] K. K. Loi, J. H. Hodiak, X. B. Mei, C. W. Tu, and W. S. C. Chang, "Linearization of 1.3 μm MQW electroabsorption modulators using an all optical frequency insensitive technique," *IEEE Photon. Technol. Lett.*, vol. 10, pp. 964–966, July 1998.
[44] K. Yamada, K. Nakamura, and H. Horikawa, "Design of double pass electroabsorption modulators with low voltage, high-speed properties for 40 Gb/s modulation," *J. Lightwave Technol.*, vol. 15, pp. 2287–2293, Dec. 1997.
[45] A. Yariv, *Introduction to Optical Electronics*, 2nd ed. New York: Holt, Rinehart and Winston, 1976.
[46] R. C. Alferness, "Waveguide electrooptic modulators," *IEEE Trans. Microwave Theory Tech.*, vol. MTT-30, pp. 1121–1137, Aug. 1982.
[47] R. Spickermann, N. Dagli, and M. G. Peters, "GaAs/AlGaAs electro-optic modulator with bandwidth $>$40 GHz," *Electron. Lett.*, vol. 31, pp. 915–917, 1995.
[48] R. Spickermann, S. R. Sakamoto, M. G. Peters, and N. Dagli, "GaAs/AlGaAs traveling wave electrooptic modulator with electrical bandwidth greater than 40 GHz," *Electron. Lett.*, vol. 32, pp. 1095–1096, 1996.
[49] G. K. Gopalakrishnan, W. K. Burns, R. W. McElhanon, C. H. Bulmer, and A. S. Greenblatt, "Performance and modeling of broad-band $LiNbO_3$ traveling-wave optical intensity modulators," *J. Lightwave Technol.*, vol. 12, pp. 1807–1819, Oct. 1994.
[50] K. Kubota, J. Noda, and O. Mikami, "Traveling-wave optical modulator using a directional coupler $LiNbO_3$ waveguide," *IEEE J. Quantum Electron.*, vol. QE-16, pp. 754–760, July 1980.
[51] I. P. Kaminow, *An Introduction to Electrooptic Devices*. New York, Academic, 1974.
[52] B. T. Szentkuti, "Simple analysis of anisotropic microstrip lines by a transform method," *Electron. Lett.*, vol. 12, pp. 672–673, 1976.
[53] K. C. Gupta, R. Garg, I. Bahl, and P. Bhartia, *Microstrip Lines and Slotlines*. Norwood, MA: Artech House, 1996.
[54] X. Zhang and T. Miyoshi, "Optimum design of coplanar waveguide for $LiNbO_3$ optical modulator," *IEEE Trans. Microwave Theory Tech.*, vol. 43, pp. 523–528, Mar. 1995.
[55] K. Noguchi, O. Mitomi, K. Kawano, and Y. Yanagibashi, "Highly efficient 40-GHz bandwidth Ti:$LiNbO_3$ optical modulator employing ridge structure," *IEEE Photon. Technol. Lett.*, vol. 5, pp. 52–54, Jan. 1993.
[56] O. Mitomi, K. Noguchi, and H. Miyazawa, "Design of ultra broad band $LiNbO_3$ optical modulators with ridge structure," *IEEE Trans. Microwave Theory Tech.*, vol. 43, pp. 2203–2207, Sept. 1995.
[57] K. Noguchi, O. Mitomi, H. Miyazawa, and S. Seki, "A broad band Ti:$LiNbO_3$ optical modulators with a ridge structure," *J. Lightwave Technol.*, vol. 13, pp. 1164–1168, June 1995.
[58] K. Noguchi, O. Mitomi, and H. Miyazawa, "Millimeter-wave Ti:$LiNbO_3$ optical modulators," *J. Lightwave Technol.*, vol. 16, pp. 615–619, Apr. 1998.
[59] K. Noguchi, H. Miyazawa, and O. Mitomi, "Frequency dependent propagation characteristics of coplanar waveguide electrode on 100 GHz Ti$LiNbO_3$ optical modulator," *Electron. Lett.*, vol. 34, no. 7, pp. 661–663, Jan. 28, 1998.
[60] G. K. Gopalakrishnan, W. K. Burns, and C. H. Bulmer, "Electrical loss mechanism in traveling wave switch/modulators," *Electron. Lett.*, vol. 28, no. 2, pp. 207–209, 1992.
[61] W. K. Burns, M. M. Howerton, R. P. Moeller, A. S. Greenblatt, and R. W. McElhanon, "Broad-band reflection traveling-wave $LiNbO_3$ modulator," *IEEE Photon. Technol. Lett.*, vol. 10, pp. 805–806, June 1998.
[62] A. M. Glass, "The photorefractive effect," *Opt. Eng.*, vol. 17, pp. 470–479, 1978.
[63] T. Fujiwara, S. Sato, and H. Mori, "Wavelength dependence of photorefractive effect in Ti indiffused $LiNbO_3$ waveguides," *Appl. Phys. Lett.*, vol. 54, pp. 975–977, 1989.
[64] G. E. Betts, F. J. O'Donnell, and K. G. Ray, "Effect of annealing photorefractive damage in titanium indiffused $LiNbO_3$ modulators," *IEEE Photon. Technol. Lett.*, vol. 6, pp. 211–213, Feb. 1994.
[65] S. K. Korotky and J. J. Veselka, "An RC network analysis of long term Ti:$LiNbO_3$ bias stability," *J. Lightwave Technol.*, vol. 14, pp. 2687–2697, Dec. 1996.
[66] H. F. Taylor, "Polarization independent guided wave optical modulators and switches," *J. Lightwave Technol.*, vol. LT-3, pp. 1277–1280, Dec. 1985.
[67] P. Granestrand, L. Thylen, and B. Stoltz, "Polarization independent switch and polarization splitter employing $\Delta\beta$ and $\Delta\kappa$ modulation," *Electron. Lett.*, vol. 24, no. 18, pp. 1142–1143, Sept. 1988.
[68] L. McCaughan, "Low loss polarization independent electrooptic switches," *J. Lightwave Technol.*, vol. LT-2, pp. 51–55, Feb. 1984.
[69] R. C. Alferness, "Polarization independent optical directional coupler switching using weighted coupling," *Appl. Phys. Lett.*, vol. 35, pp. 748–750, 1979.
[70] Y. Silberberg, P. Perlmutter, and J. E. Baran, "Digital optical switch," *Appl. Phys. Lett.*, vol. 51, no. 16, pp. 1230–1232, Oct. 1987.
[71] W. B. Bridges and J. H. Schaffner, "Distortion in linearized electrooptic modulators," *IEEE Trans. Microwave Theory Tech.*, vol. 43, pp. 2184–2197, Sept. 1995.
[72] U. V. Cummings and W. B. Bridges, "Bandwidth of linearized electrooptic modulators," *J. Lightwave Technol.*, vol. 16, pp. 1482–1490, Aug. 1998.
[73] J. G. Mendoza-Alvarez, L. A. Coldren, A. Alping, R. H. Yan, T. Hausken, K. Lee, and K. Pedrotti, "Analysis of depletion edge translation lightwave modulators," *J. Lightwave Technol.*, vol. 6, pp. 793–808, June 1998.
[74] R. G. Walker, "High-speed III–V electrooptic waveguide modulators," *IEEE J. Quantum Electron.*, vol. 27, pp. 654–667, Mar. 1991.
[75] ———, "Electro-optic modulation at mm-wave frequencies in GaAs/AlGaAs guided wave devices," in *Proc. IEEE/LEOS'95 8th Annu. Meeting*, San Francisco, CA, Oct. 30–Nov. 2, 1995, pp. 118–119.
[76] R. Spickermann, S. R. Sakamoto, M. G. Peters, and N. Dagli, "GaAs/AlGaAs traveling wave electrooptic modulator with electrical bandwidth greater than 40 GHz," *Electron. Lett.*, vol. 32, no. 12, pp. 1095–1096, June 6, 1996.
[77] R. Spickermann, S. R. Sakamoto, and N. Dagli, "GaAs/AlGaAs traveling wave electrooptic modulators," in *Proc. SPIE Optoelectron. Integrated Circuits Conf.*, vol. 3006, San Jose, CA, Feb. 8–14, 1997, pp. 272–279.
[78] S. R. Sakamoto, R. Spickermann, and N. Dagli, "Novel narrow gap coplanar slow wave electrode for traveling wave electrooptic modulators," *Electron. Lett.*, vol. 31, no. 14, pp. 1183–1185, July 6, 1995.
[79] R. Spickermann, S. R. Sakamoto, and N. Dagli, "In traveling-wave modulators which velocity to match?" in *Proc. IEEE/LEOS'96 9th Annu. Meeting*, Boston, MA, Nov. 18–21, 1996, pp. 97–98.
[80] W. W. Rigrod and I. P. Kaminow, "Wide-band microwave light modulation," *Proc. IEEE*, vol. 51, pp. 137–140, Jan. 1963.
[81] S. R. Sakamoto, C. Ozturk, Y. T. Byun, J. Ko, and N. Dagli, "Low loss substrate-removed (SURE) optical waveguides in GaAs/AlGaAs epitaxial layers embedded in organic polymers," *IEEE Photon. Technol. Lett.*, vol. 10, pp. 985–987, July 1998.
[82] J. N. Walpole, J. P. Donnelly, S. H. Groves, L. J. Missaggia, J. D. Woodhouse, R. J. Bailey, and A. Napoleone, "Diffraction limited 1.3-μm wavelength tapered gain region lasers with $>$1-W CW output power," *IEEE Photon. Technol. Lett.*, vol. 8, pp. 1429–1431, Nov. 1996.
[83] R. Spickermann, M. Peters, and N. Dagli, "A polarization independent GaAs/AlGaAs electrooptic modulator," *IEEE J. Quantum Electron.*, vol. 32, pp. 764–769, May 1996.

[84] R. Spickermann and N. Dagli, "Experimental analysis of millimeter wave coplanar waveguide slow wave structures on GaAs," *IEEE Trans. Microwave Theory Tech.*, vol. 42, pp. 1918–1924, Oct. 1994.
[85] L. A. Hornak, Ed., *Polymers for Lightwave and Integrated Optics*. New York: Marcel Dekker, 1992.
[86] S. Kalluri, M. Ziari, A. Chen, V. Chuyanov, W. H. Steir, D. Chen, B. Jalali, H. R. Fetterman, and L. R. Dalton, "Monolithic integration of waveguide polymer electrooptic modulators on VLSI circuitry," *IEEE Photon. Technol. Lett.*, vol. 8, pp. 644–646, May 1996.
[87] C. F. Kane and R. R. Krchnavek, "Benzocyclobutene optical waveguides," *IEEE Photon. Technol. Lett.*, vol. 7, pp. 535–537, May 1995.
[88] G. Fishbeck, R. Moosburger, C. Kostrzewa, A. Achen, and K. Petermann, "Single mode optical waveguides using a high temperature stable polymer with low losses in the 1.55 μm range," *Electron. Lett.*, vol. 33, no. 6, pp. 518–519, Mar. 1997.
[89] G. F. Lipscomb, A. F. Garito, and R. S. Narang, "A large linear electrooptic effect in a polar organic crystal 2-methyl-4-nitroaniline," *Appl. Phys. Lett.*, vol. 38, no. 9, pp. 663–665, 1981.
[90] D. Chen, H. Fetterman, A. Chen, W. H. Steier, L. R. Dalton, W. Wang, and Y. Shi, "Demonstration of 110 GHz electrooptic polymer modulators," *Appl. Phys. Lett.*, vol. 70, no. 25, pp. 3335–3337, 1997.
[91] D. Chen, D. Bhattacharta, A. Udupa, B. Tsap, H. Fetterman, A. Chen, S. S. Lee, J. Chen, W. H. Steier, and L. R. Dalton, "High frequency polymer modulators with integrated finline transitions and low V_π," *IEEE Photon. Technol. Lett.*, vol. 11, pp. 54–56, Jan. 1999.
[92] C. C. Teng, "Traveling wave polymeric intensity modulator with more than 40 GHz 3 dB electrical bandwidth," *Appl. Phys. Lett.*, vol. 60, pp. 1538–1540, 1992.
[93] G. D. Girton, S. L. Kwiatkowski, G. F. Lipscomb, and R. S. Lytel, "20 GHz electrooptic polymer Mach–Zehnder modulator," *Appl. Phys. Lett.*, vol. 58, pp. 1730–1732, 1991.
[94] W. Wang, Y. Shi, D. J. Olson, W. Lin, and J. Bechtel, "Push–pull poled polymer Mach–Zehnder modulators with a single microstrip line electrode," *IEEE Photon. Technol. Lett.*, vol. 11, pp. 51–53, Jan. 1999.
[95] T. T. Tumolillo and P. R. Ashley, "A novel pulse poling technique for EO polymer waveguide devices using device electrode poling," *IEEE Photon. Technol. Lett.*, vol. 4, pp. 142–145, Feb. 1992.
[96] K. H. Hahn, D. W. Dolfi, R. S. Moshrefzadeh, P. A. Pedersen, and C. V. Francis, "Novel two arm microwave transmission line for high speed electrooptic polymer modulators," *Electron. Lett.*, vol. 30, no. 15, pp. 1220–1222, July 21, 1994.
[97] Y. Shi, D. J. Olson, and J. Bechtel, "Photoinduced molecular alignment relaxation in poled electrooptic polymer thin films," *Appl. Phys. Lett.*, vol. 68, no. 8, pp. 1040–1042, 1996.
[98] M. Mortazavi, H. Yoon, and C. Teng, "Optical power handling properties of polymeric nonlinear optical waveguides," *J. Appl. Phys.*, vol. 74, pp. 4871–4876, 1993.
[99] Y. Shi, W. Wang, W. Lin, D. J. Olson, and J. H. Bechtel, "Double end cross linked electrooptic polymer modulators with high optical power handling capability," *Appl. Phys. Lett.*, vol. 70, no. 11, pp. 1342–1344, 1997.
[100] ———, "Long term stable direct current bias operation in electrooptic polymer modulators with an electrically compatible multilayer structure," *Appl. Phys. Lett.*, vol. 71, no. 16, pp. 2236–2238, 1997.
[101] H. Park, W. Y. Hwang, and J. J. Kim, "Origin of direct current drift in electrooptic polymer modulator," *Appl. Phys. Lett.*, vol. 70, no. 21, pp. 2796–2798, 1997.
[102] K. K. Loi, X. B. Mei, J. H. Hodiak, A. N. Cheng, L. Shen, H. H. Wieder, C. W. Tu, and W. S. C. Chang, "Experimental study of efficiency bandwidth tradeoff of electroabsorption waveguide modulators for microwave photonic links," in *Proc. IEEE LEOS 10th Annu. Meeting*, vol. 1, San Francisco, CA, Nov. 10–13, 1997, pp. 142–143.
[103] H. H. Liao, X. B. Mei, K. K. Loi, C. W. Tu, P. M. Asbeck, and W. S. C. Chang, "Microwave structures for traveling-wave MQW electro-absorption modulators for wide band 1.3-μm photonic links," in *Proc. SPIE, Optoelectron. Integrated Circuits*, vol. 3006, San Jose, CA, Feb. 12–14, 1997, pp. 291–300.
[104] S. Z. Zhang, Y. J. Chiu, P. Abraham, and J. E. Bowers, "25-GHz polarization insensitive electroabsorption modulators with traveling-wave electrodes," *IEEE Photon. Technol. Lett.*, vol. 11, pp. 191–193, Feb. 1999.
[105] K. Kawano, M. Kohtoku, M. Ueki, T. Ito, S. Kondoh, Y. Noguchi, and Y. Hasumi, "Polarization insensitive traveling wave electrode electroabsorption (TW-EA) modulator with bandwidth over 50 GHz and driving voltage less than 2 V," *Electron. Lett.*, vol. 33, no. 18, pp. 1580–1581, Aug. 28, 1997.

Nadir Dagli (S'77–M'87) was born in Ankara, Turkey. He received the B.S. and M.S. degrees in electrical engineering from the Middle East Technical University, Ankara, Turkey in 1976 and 1979, respectively, and Ph.D. degree in electrical engineering from Massachusetts Institute of Technology, Cambridge, in 1987.

During his Ph.D. research, he worked on the design, fabrication, and modeling of guided-wave integrated optical components in III–V compound semiconductors. He also worked on III–V materials preparation by liquid phase epitaxy (LPE) and the modeling and analysis of heterojunction bipolar transistors for microwave and millimeter-wave applications. Following graduation, he joined the Electrical and Computer Engineering Department, University of California at Santa Barbara, where he is currently a Professor. He has authored and co-authored over 100 publications in refereed journals and conferences. His current interests are design, fabrication, and modeling of guided-wave components for optical integrated circuits, ultrafast electrooptic modulators and wavelength division multiplexing (WDM) components, calculations on the optical properties of quantum wires, and experimental study of novel quantum devices based on ballistic transport in quantum wires.

Dr. Dagli was a member of the Subcommittee on Modeling, Numerical Simulation and Theory of Integrated Photonics Research Topical Meeting (IPR) (1992–1995), and chaired the same subcommittee in 1994. He was the program co-chair of IPR'98, and is the chair of IPR'99. From 1994 to 1998, he served on the editorial board of IEEE TRANSACTIONS ON MICROWAVE THEORY AND TECHNIQUES and as a member of the Integrated Optics and Optoelectronics Committee of the IEEE Lasers and Electro-Optics Society (LEOS) Annual Meeting. He also served as a program committee member for the IEEE Microwave Photonics'97 Conference, and was the program co-chair of the IEEE Microwave Photonics'98 Conference. He was a co-organizer of the optoelectronics session of the 1996 Workshop on Compound Semiconductors and Devices (WOCSEMMAD'96). He is also a member of the program committee of Optoelectronic Integrated Circuits Conference, which is part of SPIE's Photonics West'97 International Symposium. In this conference, he organized a session on high-speed modulators. He is currently also serving on the microoptics, integrated, and guided-wave optics technical committee of the 1999 CLEO/Pacific Rim Conference. He is an associate editor for the IEEE PHOTONICS TECHNOLOGY LETTERS. He was awarded NATO science and IBM pre-doctoral fellowships during his graduate studies. He was the recipient of 1990 University of California at Santa Barbara Alumni Distinguished Teaching Award and a 1990 University of California Regents Junior Faculty Fellowship.